bioRxiv preprint doi: https://doi.org/10.1101/2019.12.16.877605; this version posted December 17, 2019. The copyright holder for this preprint (which was not certified by peer review) is the author/funder. All rights reserved. No reuse allowed without permission.

Bacterial cell wall integrity surveillance is connected to peptidoglycan biosynthesis by the essential phosphorylation of ReoM

Sabrina Wamp[a], Zoe J.Rutter[b], Jeanine Rismondo[a,c], Claire E. Jennings[d], Lars Möller[e], Richard J. Lewis[b] and Sven Halbedel[a,*]

[a] FG11 - Division of Enteropathogenic bacteria and *Legionella*, Robert Koch Institute, Burgstrasse 37, 38855 Wernigerode, Germany;
[b] Institute for Cell and Molecular Biosciences, Medical School, University of Newcastle, Catherine Cookson Building, Framlington Place, Newcastle upon Tyne NE2 4HH, UK NE2 4HH, United Kingdom;
[c] Section of Microbiology and MRC Centre for Molecular Bacteriology and Infection, Imperial College London, London SW7 2AZ, United Kingdom;
[d] Newcastle Drug Discovery, Northern Institute for Cancer Research, Paul O'Gorman Building, Medical School, Framlington Place, Newcastle upon Tyne NE2 4HH, UK.
[e] ZBS 4 - Advanced Light and Electron Microscopy, Robert Koch Institute, Seestraße 10, 13353 Berlin, Germany;

[*] Corresponding author:

halbedels@rki.de, Robert Koch Institute, FG11 - Division of Enteropathogenic bacteria and *Legionella*, Burgstrasse 37, 38855 Wernigerode, Germany; phone: +49-30-18754-4323; fax: +49-30-18754-4207;

Keywords: PASTA-domain, serine/threonine protein kinase, peptidoglycan, protein degradation, ClpCP protease

bioRxiv preprint doi: https://doi.org/10.1101/2019.12.16.877605; this version posted December 17, 2019. The copyright holder for this preprint (which was not certified by peer review) is the author/funder. All rights reserved. No reuse allowed without permission.

ABSTRACT

Peptidoglycan (PG) is the main component of bacterial cell walls and the target for many antibiotics. PG biosynthesis is tightly coordinated with cell wall growth and turnover and many of these control activities depend upon PASTA-domain containing eukaryotic-like serine/threonine protein kinases (PASTA-eSTK) that sense PG fragments. However, only a few PG biosynthetic enzymes are actually direct kinase substrates. Here, we identify the conserved ReoM protein as a novel PASTA-eSTK substrate in the Gram-positive pathogen *Listeria monocytogenes*. Our data show that the phosphorylation of ReoM is essential as it controls ClpCP-dependent proteolytic degradation of the essential enzyme MurA, which catalyses the first committed step in PG biosynthesis. We also identify ReoY as a second novel factor required for degradation of ClpCP substrates. Collectively, our data imply that the first committed step of PG biosynthesis is activated through control of ClpCP protease activity in response to signals of PG homeostasis imbalance.

bioRxiv preprint doi: https://doi.org/10.1101/2019.12.16.877605; this version posted December 17, 2019. The copyright holder for this preprint (which was not certified by peer review) is the author/funder. All rights reserved. No reuse allowed without permission.

INTRODUCTION

The cell wall of Gram-positive bacteria is a complicated three-dimensional structure that engulfs the cell as a closed sacculus. The main component of bacterial cell walls is peptidoglycan (PG), a network of glycan strands crosslinked together by short peptides (1). PG biosynthesis starts with the conversion of UDP-Glc*N*Ac into lipid II, a disaccharide pentapeptide that is ligated to a membrane-embedded bactoprenol carrier lipid (2). This monomeric PG precursor is then flipped from the inner to the outer leaflet of the cytoplasmic membrane by MurJ- and Amj-like enzymes called flippases (3-5). Glycosyltransferases belonging either to the bifunctional penicillin binding proteins (PBPs) or the recently identified SEDS (shape, elongation, division and sporulation) family then transfer the disaccharide pentapeptides to growing PG strands, which are crosslinked by a transpeptidation reaction catalysed by monofunctional (class B) or bifunctional (class A) PBPs (6-9). Numerous hydrolytic or PG-modifying enzymes are also required to adapt the sacculus to the morphological changes that occur during bacterial cell growth and division (10, 11) or to alter its chemical properties for instance for immune evasion (12). Finally, a suite of regulators ensure that spatiotemporal control of PG synthesis is balanced against PG hydrolysis in cycles of bacterial growth and division (13).

The activity of several key enzymes along the PG biosynthetic pathway is regulated by PASTA (PBP and serine/threonine kinase associated) domain-containing eukaryotic-like serine/threonine protein kinases (PASTA-eSTKs) (14-16). These membrane-integral enzymes comprise a cytoplasmic kinase domain linked to several extracellular PASTA domains by a single transmembrane region (15). The kinase activity is stimulated by free muropeptides and lipid II (that accumulate during damage and turnover of PG) on interaction with the PASTA domains (17, 18). PknB, a representative of this protein family from *Mycobacterium tuberculosis*,

bioRxiv preprint doi: https://doi.org/10.1101/2019.12.16.877605; this version posted December 17, 2019. The copyright holder for this preprint (which was not certified by peer review) is the author/funder. All rights reserved. No reuse allowed without permission.

phosphorylates GlmU, a bifunctional uridyltransferase/acetyltransferase important for synthesis of UDP-Glc*N*Ac, and in so doing reduces GlmU activity (19). *M. tuberculosis* MviN, a MurJ-like flippase, is also a substrate of PknB and, in its phosphorylated state, P-MviN forms inhibitory complexes with its binding partner FhaA (20). *M. tuberculosis* PknB also phosphorylates both the class A PBP PonA1 (21) and the amidase-like PG-hydrolase CwlM, which is essential for growth (22-24). CwlM is membrane-associated and interacts with MurJ to control lipid II export (24). However, when phosphorylated, P-CwlM re-locates from the membrane to the cytoplasm (24) where it allosterically activates MurA 20–40-fold (23). MurA catalyzes the first committed step of PG biosynthesis by transferring an enoylpyruvate moiety to UDP-Glc*N*Ac; MurA is essential in *M. tuberculosis* and in all other bacterial species tested (25-28). Finally, the *Listeria monocytogenes* PASTA-eSTK, PrkA, phosphorylates YvcK, which is required for cell wall homeostasis, and both proteins are important for the survival of this facultative intracellular pathogen inside the cytosol of infected host cells (29).

Numerous additional proteins acting to coordinate cell wall biosynthesis with cell division are substrates of PASTA-eSTKs in other Gram-positive bacteria (15), including the late cell division protein GpsB, which is reported to be phosphorylated by PrkC, the PASTA-eSTK of *Bacillus subtilis* (30, 31). We have shown previously that GpsB from *L. monocytogenes* is important for the last two steps of PG biosynthesis, *i. e.* transglycosylation and transpeptidation, by providing an assembly platform for the class A PBP, PBP A1 (32-35), and this adaptor function of GpsB is maintained in at least *B. subtilis* and *Streptococcus pneumoniae* (34). An *L. monocytogenes* Δ*gpsB* mutant is impaired in PG biosynthesis and cannot grow at elevated temperatures (32), but this phenotype is readily corrected by a suppressor mutation, which mapped to *clpC* (28). ClpC is the ATPase subunit of the ClpCP protease molecular machine that degrades substrate proteins upon heat stress (36). MurA (*aka* MurAA in *B. subtilis*) is a ClpCP substrate in both *B. subtilis*

bioRxiv preprint doi: https://doi.org/10.1101/2019.12.16.877605; this version posted December 17, 2019. The copyright holder for this preprint (which was not certified by peer review) is the author/funder. All rights reserved. No reuse allowed without permission.

and *L. monocytogenes* (26, 28) and strongly accumulates in a *L. monocytogenes* Δ*clpC* mutant (28). Thus, a deficiency in the final two enzymatic steps of PG biosynthesis in the absence of GpsB is corrected by mutations in *clpC* that increase the amount of the first enzyme of the same PG biosynthetic pathway.

Here we isolate novel *gpsB* suppressor mutations affecting *Listeria* genes previously unstudied. We demonstrate that both proteins control the ClpCP-dependent degradation of MurA in a PrkA-dependent and hitherto unprecedented manner. One of them is phosphorylated by PrkA and this phosphorylation is essential. With these observations, we present the first molecular link between PrkA-dependent cell wall integrity sensing and control of PG production in low G/C Gram-positive bacteria, which explains how PG biosynthesis is adjusted in these bacteria to meet PG production and repair needs.

bioRxiv preprint doi: https://doi.org/10.1101/2019.12.16.877605; this version posted December 17, 2019. The copyright holder for this preprint (which was not certified by peer review) is the author/funder. All rights reserved. No reuse allowed without permission.

RESULTS

Novel *gpsB* suppressor mutations in the *lmo1503* (*reoM*) and *lmo1921* (*reoY*) genes

A *L. monocytogenes* Δ*gpsB* mutant is unable to replicate at 42°C but forms suppressors correcting this defect with high frequency (28). In a preliminary selection of *gpsB* suppressors, the *clpC* and *murZ* genes, important for the stability of the UDP-*N*-acetylglucosamine 1-carboxyvinyltransferase MurA, were found to be mutated (28). We have characterized three more *shg* (suppression of heat sensitive growth) suppressor mutants (*shg8*, *shg10* and *shg12*) isolated from a Δ*gpsB* mutant incubated on a BHI agar plate at 42°C. These three *shg* strains grew as fast as the wild type when cultivated at 37°C or 42°C, whereas the parental Δ*gpsB* mutant grew at a reduced rate at 37°C and did not grow at 42°C (Fig. 1A-B), as shown previously (32).

Illumina sequencing of the *shg8*, *shg10* and *shg12* genomes identified one SNP in each strain that was not found in the parental Δ*gpsB* strain. Strain *shg8* carried a mutation in the uncharacterized *lmo1921* gene (herein named *reoY*, see below) that exchanged H87 into tyrosine; the same gene was affected by the introduction of a premature stop codon after the 73rd codon of *reoY* to yield strain *shg10*. Strain *shg12* carried a mutation in the ribosomal binding site (RBS) of the *lmo1503* gene (renamed *reoM*), encoding another protein of unknown function and containing a DUF956 domain, widely conserved in bacteria but with no function ascribed.

Whether the mutation in the RBS of *reoM* in strain *shg12* led to its inactivation, expression effects or a gain of function was not clear. Therefore, the *reoM* gene was deleted from the genome of the wild type strain and the Δ*gpsB* mutant. While deletion of *reoM* had no effect on growth of wild type bacteria, it suppressed completely the growth defects of the Δ*gpsB* mutant at both 37°C and 42°C (Fig. 1C-D). It is thus likely that the mutation in the *reoM* RBS impairs its

bioRxiv preprint doi: https://doi.org/10.1101/2019.12.16.877605; this version posted December 17, 2019. The copyright holder for this preprint (which was not certified by peer review) is the author/funder. All rights reserved. No reuse allowed without permission.

127 expression. Likewise, deletion of *reoY* led to the complete restoration of growth in the Δ*gpsB*
128 Δ*reoY* double mutant at both 37°C and 42°C (Fig. 1C-D).
129 Expression of an additional, plasmid-borne copy of *reoM* impaired growth of the Δ*gpsB* mutant
130 without affecting the growth of wild type bacteria, whilst expression of a second copy of *reoY*
131 had no effect (Fig. S1A,B). The expression of *reoM* is thus inversely correlated with the growth
132 of the Δ*gpsB* mutant. To further validate these conclusions, the genomes of the Δ*reoM* and Δ*reoY*
133 single and the Δ*gpsB* Δ*reoM* and Δ*gpsB* Δ*reoY* double mutants were analysed by Illumina
134 sequencing. No additional mutations were found in any of these strains, confirming that the *reoM*
135 and *reoY* deletions were the sole reason for the suppression of the Δ*gpsB* phenotype.
136 Finally, the physiology of the strains harbouring novel *gpsB* suppressor genes was examined. The
137 cell lengths of strains lacking *reoM* and *reoY* were unaffected by the presence or absence of *gpsB*,
138 and were the same as the wild type strain, suggesting the absence of cell division defects in the
139 Δ*reoM* or Δ*reoY* mutants (Fig. S2A,B). Furthermore, scanning electron micrographs of Δ*reoM*
140 and Δ*reoY* single mutants revealed that these bacteria had a normal rod-shape, but that the Δ*gpsB*
141 Δ*reoM* and Δ*gpsB* Δ*reoY* double mutants were partially bent (Fig. S2C), implying the presence
142 of shape maintenance defects along the lateral cell cylinders.
143
144 **ReoM and ReoY affect the stability of MurA**
145 Suppression of the Δ*gpsB* phenotype can be achieved by the accumulation of the UDP-*N*-
146 acetylglucosamine 1-carboxyvinyltransferase MurA (28). Consequently, MurA levels were
147 determined in Δ*reoM* and Δ*reoY* mutant strains by Western blotting. MurA accumulated by at
148 least eight-fold in comparison to the wildtype in the absence of *reoM* or *reoY* (Fig. 2A),
149 indicating that the Δ*gpsB* suppression involves MurA accumulation in Δ*reoM* and Δ*reoY*
150 mutants. Remarkably, MurA accumulation in Δ*reoM* and Δ*reoY* mutants reached similar levels as

bioRxiv preprint doi: https://doi.org/10.1101/2019.12.16.877605; this version posted December 17, 2019. The copyright holder for this preprint (which was not certified by peer review) is the author/funder. All rights reserved. No reuse allowed without permission.

in a mutant lacking *clpC*, which encodes the ATPase subunit of the ClpCP protease (Fig. 2A). Both MurAA, the *B. subtilis* MurA homologue, and *L. monocytogenes* MurA are degraded by their respective ClpCP proteases *in vivo* (26, 28). In order to test whether *reoM* and *reoY* exert their effect on MurA in a ClpC-dependent manner, MurA levels were determined in Δ*clpC* Δ*reoM* and Δ*clpC* Δ*reoY* double mutants. The MurA levels in Δ*clpC*, Δ*reoM* and Δ*reoY* single mutants were the same as in Δ*clpC* Δ*reoM* and Δ*clpC* Δ*reoY* double mutant strains (Fig. 2B). Likewise, the MurA level in a mutant lacking *murZ*, previously shown to contribute to MurA stability (28), is not additive to the MurA level in Δ*clpC* cells (Fig. 2B). Therefore, *reoM*, *reoY* and *murZ* likely affect the ClpCP-dependent degradation of MurA and each are thus important for the stability of MurA against targeted proteolytic degradation. Moreover, combinations of Δ*reoM*, Δ*reoY* and Δ*murZ* deletions did not exert any additive effect on accumulation of MurA (Fig. S3A,B) further validating the conclusion that these genes all belong to the same pathway.

The effect of ReoM and ReoY on MurA levels is conserved

Homologues of the 90-residue ReoM protein are found across the entire Firmicute phylum, and include IreB, a substrate of the protein serine/threonine kinase IreK and its cognate phosphatase IreP from *Enterococcus faecalis* (37), whereas ReoY homologues are present only in the *Bacilli*. In *B. subtilis*, ReoM corresponds to YrzL (e-value $3e^{-29}$) and ReoY to YpiB ($4e^{-61}$), but neither protein has been studied thus far. Analysis of the chromosomal structure reveals that *yrzL* is in an operon with *alaS*, *yrrK* and *yrzB* (38) and expression seems to be regulated by an alanine-dependent T-box (39). YrrK seems to be an RNAse that degrades the 5'-end of 16S rRNA (40). It is perhaps pertinent to note that just 9 genes downstream are the PBPI (aka PBP4) and YrrS reading frames, both of which are binding partners of GpsB (34). By contrast, expression of *ypiB* was reported to be under the control of σ^H (41). To assess whether YrzL and YpiB were also

bioRxiv preprint doi: https://doi.org/10.1101/2019.12.16.877605; this version posted December 17, 2019. The copyright holder for this preprint (which was not certified by peer review) is the author/funder. All rights reserved. No reuse allowed without permission.

crucial for control of MurAA levels in *B. subtilis*, cellular protein extracts from *B. subtilis* Δ*yrzL* and Δ*ypiB* mutants were probed by Western blot (Fig. 2C). MurAA accumulated by at least 12-fold in these strains in comparison to the wildtype. Furthermore, the amount of MurAA was also increased by 12-fold in the Δ*clpC* mutant. Taken together, these data indicate that ReoM and ReoY functions are conserved in both species implying that homologues of these proteins exert similar effects on MurA levels in all other Firmicutes. We thus propose to rename *lmo1503* (*yrzL*) as *reoM* (regulator of MurA(A) degradation) and analogously *lmo1921* (*ypiB*) as *reoY*.

Several other ClpC substrates are known in *B. subtilis*, including the glutamine fructose-6-phosphate transaminase GlmS and the acetolactate synthase subunit IlvB (42). The levels of both proteins were significantly increased in *B. subtilis* Δ*reoM* and Δ*reoY* mutants (Fig. S4), indicating that ReoM and ReoY are required for degradation of ClpC substrates in general.

Phosphorylation and dephosphorylation of ReoM by PrkA and PrkP i*n vitro*

PrkA (encoded by *lmo1820*) and PrkP (*lmo1821*) are the *L. monocytogenes* homologs of *E. faecalis* IreK and IreP, respectively. Consequently, the pairwise interactions and biochemical properties of ReoM, the PrkA kinase domain (PrkA-KD) and the cognate phosphatase PrkP were investigated. All isolated proteins electrophoresed as single species in non-denaturing PAGE (lanes 1, 2, Fig. 3A; lanes 1-4, Fig. 3B). When ReoM was incubated with PrkA-KD, in the absence of ATP, a slower migrating species was observed and the individual bands corresponding to ReoM and PrkA-KD disappeared indicating that the slower migrating species was a ReoM:PrkA-KD complex (lane 3, Fig. 3A). When ReoM was incubated with PrkA-KD and Mg/ATP under the same conditions, free PrkA-KD was observed but no bands equivalent to ReoM and the ReoM:PrkA-KD complex remained; instead a new species was present, migrating faster in the gel than ReoM (lane 4, Fig. 3A), which is likely to be phosphorylated ReoM (P-

bioRxiv preprint doi: https://doi.org/10.1101/2019.12.16.877605; this version posted December 17, 2019. The copyright holder for this preprint (which was not certified by peer review) is the author/funder. All rights reserved. No reuse allowed without permission.

ReoM). Intact protein liquid chromatography-mass spectrometry (LC-MS) analysis of ReoM isolated from PrkA-KD after phosphorylation revealed the addition of 79.9 Da in comparison to the mass of ReoM (10671.5 Da), which corresponds to the formation of a singly-phosphorylated ReoM product of 10751.4 Da (Fig. 3C, S5). MS/MS spectra obtained during peptide mass fingerprinting were also consistent with one phosphorylation event per protein chain: the mass of one ReoM peptide, spanning residues Asp5 to Lys22 with mass of 2151.89 Da, was increased by 79.96 Da after incubation with PrkA-KD and Mg/ATP. Analysis of the *y*- and *b*- ions in the MS/MS fragmentation spectrum of this peptide was consistent only with Thr7 as the sole phosphosite in ReoM (Fig. 3D). Finally, mutation of Thr7 to alanine completely abrogated the phosphorylation of ReoM by PrkA-KD when analysed by LC-MS (Fig. S6).

The ability of PrkP, the partner phosphatase to PrkA in *L. monocytogenes*, to interact with and remove phosphoryl groups from PrkA-KD and P-ReoM was also tested *in vitro*. PrkA and purified P-ReoM were each incubated with PrkP in the absence and presence of $MnCl_2$, since divalent cations are essential co-factors for the PPM phosphatase family to which PrkP belongs (43), and the products were analysed by non-denaturing PAGE. Unlike the situation with ReoM and PrkA-KD, no stable protein:protein complexes were formed either in the presence or absence of endogenous $MnCl_2$ (Fig. 3B). The incubation of P-ReoM with PrkP and manganese resulted in the almost complete disappearance of the band corresponding to P-ReoM (lane 6, Fig. 3B) in comparison to the same reaction conducted without the addition of $MnCl_2$ (lane 5, Fig. 3B). The new band, corresponding to ReoM alone in lane 6, is masked by that for PrkP which migrates similarly to ReoM (lanes 1 and 4, Fig. 3B) under these electrophoresis conditions, but the presence of unphosphorylated ReoM and the absence of P-ReoM was confirmed by LC-MS (Fig. S7). When incubated with PrkP in the presence of manganese ions, the band for PrkA-KD electrophoresed more slowly than for PrkA-KD in isolation (lanes 3 and 8, Fig. 3B), indicating

bioRxiv preprint doi: https://doi.org/10.1101/2019.12.16.877605; this version posted December 17, 2019. The copyright holder for this preprint (which was not certified by peer review) is the author/funder. All rights reserved. No reuse allowed without permission.

that PrkA-KD had been dephosphorylated by PrkP. LC-MS analysis of PrkA-KD that had been incubated with PrkP/$MnCl_2$ yielded a single major species of 37,413.2 Da, consistent with the predicted mass of the expressed recombinant construct, and the absence of a peak corresponding to phosphorylated PrkA-KD, P-PrkA-KD (Fig. S8). Therefore, PrkA-KD is capable of autophosphorylation even when expressed in a heterologous host, consistent with previous observations made for similar PASTA-eSTKs from other Gram-positive bacteria (44, 45). Finally, in the absence of $MnCl_2$ no change in electrophoretic mobility was observed for P-PrkA-KD (lane 7, Fig. 3B).

Phosphorylation of ReoM at threonine 7 is essential for viability

PrkA phosphorylates ReoM on Thr7 and PrkP reverses this reaction. In the absence of molecular details on the impact of Thr7 phosphorylation we determined the importance of this phosphorylation *in vivo* by engineering a phospho-ablative T7A exchange in an IPTG-inducible allele of *reoM* and introduced it into the Δ*reoM* mutant background. Deletion, depletion or expression of wildtype *reoM* had no effect on growth in strains LMSW30 (Δ*reoM*) and LMSW57 (i*reoM*, i - is used to denote IPTG-dependent alleles throughout the manuscript) at 37°C. Likewise, strain LMSW52 (i*reoM T7A*) grew normally in the absence of IPTG. However, the *reoM* mutant with the T7A mutation did not grow at all in the presence of IPTG, when expression of the phospho-ablative *reoM* T7A allele was induced (Fig. 4A), suggesting that phosphorylation of ReoM at Thr7 is essential for the viability of *L. monocytogenes*. Since ReoM influences the proteolytic stability of MurA, we determined the cellular amount of MurA in strains expressing the T7A variant of ReoM. For this purpose, strains LMSW57 (i*reoM*) and LMSW52 (i*reoM T7A*) were initially cultivated in plain BHI broth. At an OD_{600} of 0.2, IPTG was added to a final concentration of 1 mM and cells were harvested 2 hours later. Strain LMSW57 (i*reoM*) showed

bioRxiv preprint doi: https://doi.org/10.1101/2019.12.16.877605; this version posted December 17, 2019. The copyright holder for this preprint (which was not certified by peer review) is the author/funder. All rights reserved. No reuse allowed without permission.

247 Δ*clpC*-like MurA accumulation (around seven-fold in this experiment) when cultured in the
248 absence of IPTG, but MurA was present at wild type levels in the presence of IPTG (Fig. 4C).
249 The strain with the T7A exchange also accumulated MurA to a Δ*clpC*-like extent in the absence
250 of IPTG. However, around 10% of the wild type MurA levels could be detected in cells
251 expressing the *reoM T7A* allele (Fig. 4C). These data demonstrate that Thr7 in ReoM is of special
252 importance for the proteolytic stability of MurA.
253
254 **Lethality of the *reoM T7A* mutations depends on ClpC**
255 That MurA is rapidly degraded in cells expressing *reoM T7A* implies that
256 phosphorylation/dephosphorylation of ReoM at Thr7 controls ClpCP-dependent MurA
257 degradation. MurA is an essential enzyme in *L. monocytogenes* (28), and stimulation of ClpCP-
258 dependent MurA degradation in the *reoM T7A* mutant would provide an explanation for the
259 lethality of this mutation. In order to address this possibility, we deleted *clpC* in the conditional
260 i*reoM T7A* background. This strain grew even in the presence of IPTG, a compelling
261 demonstration that the removal of *clpC* suppressed the lethality of the *reoM T7A* mutation (Fig.
262 4B). MurA also accumulated to the same degree as in the Δ*clpC* mutant in this strain (Fig. 4C),
263 suggesting that inactivation of the ClpCP-dependent degradation of MurA overcame the lethal
264 effect of the T7 mutation in *reoM*. Moreover, this suggests that ClpCP acts downstream of ReoM.
265 We next wondered whether deletion of *reoY* and *murZ* would have a similar effect and also
266 deleted these genes in the *reoM T7A* mutant. As can be seen in Fig. 4D, deletion of either gene
267 also overcame the lethality of *reoM T7A*, indicating that ReoY and MurZ must also act
268 downstream of ReoM.

bioRxiv preprint doi: https://doi.org/10.1101/2019.12.16.877605; this version posted December 17, 2019. The copyright holder for this preprint (which was not certified by peer review) is the author/funder. All rights reserved. No reuse allowed without permission.

Crystal structure of ReoM, a homologue of *Enterococcus faecalis* IreB

Purified ReoM yielded crystals that diffracted to a maximum resolution of 1.6 Å. The structure of IreB (PDBid 5US5) (46) was used to solve the structure of ReoM by molecular replacement (Fig. 5A). The data collection and refinement statistics for the ReoM structure are summarised in Table 3. ReoM shares the same overall fold as IreB (46), each containing a compact 5-helical bundle (4 standard α-helices and one single-turned 3_{10}-helix between residues 52 and 54) with short loops between the secondary structure elements, which are defined above the sequence alignment in Fig. 5B. Other than IreB (46), there are no functionally-significant structural homologues of ReoM in the PDB. In both cases the helical bundles associate into homodimers with α-helices two and four from each protomer forming the majority of the homodimer interface (Fig. 5A), and these residues are highlighted in Fig. 5B. In agreement with the IreB structural analysis, 1200 $Å^2$ of surface area is buried in the ReoM dimer interface, representing 9% of the total solvent accessible surface area. The similarity of the monomers and the dimeric assemblies of ReoM and IreB is underlined by the 1.5 and 1.7 Å r.m.s.d. values, respectively, on global secondary structure superposition matching 74 Cα atoms from each protomer in the comparison.

Other than the compact helical bundle of ReoM, there is a ~16 residue-long N-terminal tail, with B-factors 25% higher than the rest of the protein, prior to the start of α-helix 1 at residue Ile17. The equivalent N-terminal region is also disordered in the NMR structure of IreB (46). Despite the absence of secondary structure, the ReoM model covering this region could be built with confidence from Asp5 in chain A and Asp2 in chain B (Fig. 5C). Consequently, it is possible to visualise Thr7, the target for phosphorylation by PrkA, in the flexible N-terminal region in both chains. The side chain of Thr7 in both chains makes no intramolecular interactions and is thus amenable to phosphorylation by PrkA. The extended N-terminal regions are at least partially stabilised by crystal lattice interactions that, in chain B, include Phe9 and Tyr10 forming a

bioRxiv preprint doi: https://doi.org/10.1101/2019.12.16.877605; this version posted December 17, 2019. The copyright holder for this preprint (which was not certified by peer review) is the author/funder. All rights reserved. No reuse allowed without permission.

network of hydrophobic interactions with other aromatic residues from symmetry equivalent molecules, including contributions from another copy of Phe9 and Tyr10. Phosphorylation could force a change in oligomeric state, as observed quite commonly in response regulators in order to bind more effectively to promoter regions to effect transcription (47). However, analysis of the oligomeric state of P-ReoM by size exclusion chromatography revealed that the protein behaved in solution the same as to unphosphorylated ReoM (Fig. S9).

Unlike the packing arrangement of Thr7 in chain B, the local symmetry surrounding Thr7 in chain A might provide some information of potential functional significance to the phosphorylated form of ReoM. Here, a sulphate ion (a component of the crystallisation reagent) is hydrogen bonded to the sidechain of Thr7 and hence mimics, to some degree, what the phosphorylated protein may look like (Fig. 5C). The sulphate ion is captured by a positively-charged micro-environment incorporating residues Lys35, Arg57, His58 and Arg62 from a symmetry-equivalent molecule. Intramolecular re-arrangements of structures to accommodate phosphorylated amino acids in positively-charged surface environments is a common response to phosphorylation, with distances of up to 50 Å between the positions of phosphorylated and non-phosphorylated Ser14 in rabbit muscle glycogen phosphorylase, for example (47). ReoM could react to phosphorylation on Thr7 by a substantial movement of the N-terminal tail to interact with conserved, positively-charged amino acids on the protein surface. We identified a single cluster of arginines (Arg57 [57%], Arg62 [99%], Arg66 [76%], Arg70 [98%]) in close spatial proximity with levels of conservation amongst all 2909 ReoM homologues present at NCBI approaching that of Thr7 (96%). Alanine substitutions were made at these four positions and the respective mutated alleles were expressed in the *L. monocytogenes* Δ*reoM* background. Whereas the R66A and R70A mutations were without any effect on growth (data not shown), expression of ReoM R57A and R62A mutations were as lethal as expression of ReoM T7A (Fig. S10). Thus, Arg57

bioRxiv preprint doi: https://doi.org/10.1101/2019.12.16.877605; this version posted December 17, 2019. The copyright holder for this preprint (which was not certified by peer review) is the author/funder. All rights reserved. No reuse allowed without permission.

and Arg62 might co-ordinate P-Thr7, stabilising the conformation and position of the flexible N-terminal region (Fig. S11), leading to a change in the surface electrophysical properties of ReoM to drive the downstream consequences of its phosphorylation. Despite multiple attempts no crystals were grown of P-ReoM and, therefore, the molecular consequences of ReoM phosphorylation remains to be determined.

Control of MurA stability by the PrkA/PrkP protein kinase/phosphatase pair

To study the contribution of the PrkA/PrkP couple to cell wall biosynthesis in more detail, we aimed to construct *prkA* and *prkP* deletion mutants, but failed to delete *prkA*, as has been reported previously (29). However, *prkA* could be deleted in the presence of an IPTG-inducible ectopic *prkA* copy and the resulting strain (LMSW84) required IPTG for growth (Fig. 6A), demonstrating the essentiality of this gene. Repeated attempts to delete *prkP* finally yielded a single Δ*prkP* clone (LMSW76). Genomic sequencing of this strain, which grew at a similar rate to wildtype (Fig. 6A), confirmed the successful deletion of *prkP* but also identified a trinucleotide deletion in the *prkA* gene (designated *prkA**), effectively removing the complete codon of Gly18 that is part of a conserved glycine-rich loop important for ATP binding (48). Presumably, this mutation reduces the PrkA kinase activity to balance the absence of PrkP. By contrast, *prkP* could be deleted readily in the presence of a second IPTG-dependent copy of *prkP* and growth of the resulting strain (LMSW83) did not require IPTG, most likely explained by promoter leakiness in the absence of IPTG (Fig. 6A). Next, the effect of *prkA* and *prkP* mutations on MurA accumulation was analyzed by Western blotting. Intermediate MurA accumulation was evident in the Δ*prkP prkA** strain, while full accumulation of MurA was observed in PrkP-depleted cells. By contrast, no MurA was detected in cells depleted for PrkA (Fig. 6B). Therefore, PrkA and

bioRxiv preprint doi: https://doi.org/10.1101/2019.12.16.877605; this version posted December 17, 2019. The copyright holder for this preprint (which was not certified by peer review) is the author/funder. All rights reserved. No reuse allowed without permission.

PrkP inversely contribute to the accumulation of MurA suggesting that phosphorylated ReoM favors MurA accumulation, while un-phosphorylated ReoM counteracts this process.

Deletion of *reoM*, *reoY* or *clpC* eliminates *prkA* essentiality

In order to test whether the essentiality of *prkA* could be explained by complete MurA degradation through ClpCP, we first tested the effect of *clpC* on the essentiality of *prkA*. For this purpose, *clpC* was removed from the i*prkA* strain and growth of the resulting strain (LMSW91) was tested. In contrast to the parental i*prkA* strain (LMSW84), which required IPTG for growth, strain LMSW91 was viable without IPTG (Fig. 7A), confirming that the essentiality of PrkA depends on ClpC. As we have shown above, ReoM controls MurA stability via ClpC and is phosphorylated by PrkA (Fig. 2B and 3A). Thus, we wondered whether ReoM was required for PrkA essentiality and consequently deleted *reoM* from the i*prkA* background to test this hypothesis. Again, the resulting strain (LMSW89) did not require IPTG for growth in contrast to the parental i*prkA* strain (Fig. 7A). Finally, we tested the contribution of *reoY* to *prkA* essentiality in a similar manner and also found that deletion of *reoY* suppressed the essentiality of *prkA* (Fig. 7A). In good agreement with these findings, deletion of *clpC*, *reoM* or *reoY* all stabilized MurA in PrkA-depleted cells (Fig. 7B), showing that the stimulated degradation of MurA that we observe in cells depleted for PrkA (Fig. 6B) is dependent on any one of these three proteins. These results indicate that the essentiality of PrkA is explained by its contribution to proteolytic stabilization of another essential enzyme, MurA, and since ReoM and ReoY play a crucial role in this process, their deletion has the same effect on suppression of the Δ*gpsB* phenotype as the deletion of *clpC*.

bioRxiv preprint doi: https://doi.org/10.1101/2019.12.16.877605; this version posted December 17, 2019. The copyright holder for this preprint (which was not certified by peer review) is the author/funder. All rights reserved. No reuse allowed without permission.

DISCUSSION

With ReoM we have identified a missing link in a regulatory pathway that enables Firmicute bacteria to activate PG biosynthesis under conditions damaging their cell walls. In *L. monocytogenes*, the sensory module of this pathway comprises the membrane integral protein kinase PrkA and the cognate protein phosphatase PrkP, their newly discovered substrate ReoM and the associated factors ReoY and MurZ, which together regulate ClpCP activity, the effector protease that acts on MurA (Fig. 8). It has been demonstrated previously that the kinase activity of PrkA homologues was activated by muropeptides (17, 49) or the PG precursor lipid II (18). Muropeptides were released from the cell wall during normal PG turnover, and their release was intensified when PG hydrolysis prevailed over PG biosynthesis (10, 50), whereas blocking PG chain elongation by moenomycin treatment caused the accumulation of lipid-linked PG precursors (51). Thus, both types of molecules accumulated when PG biosynthesis was inhibited and could represent useful signals for detecting cell wall-damaging situations. We show here that upon stimulation, PrkA phosphorylated ReoM and P-ReoM no longer activates ClpCP, which leads to MurA stabilization and activation of PG biosynthesis (Fig. 8).

How ReoM and ReoY exert their effect on ClpCP is currently unknown, but a fascinating possibility would be a function similar to that of an adaptor protein to target a subset of protein substrates, including MurA, to the ClpCP complex for degradation. Several ClpC adaptors are known in *B. subtilis* (52, 53), but an adaptor for *Bs*MurAA is not among them (26, 52). Interestingly, the ClpC adaptor protein McsB from *B. subtilis* is also subject to phosphorylation like ReoM but, unlike ReoM, it targets its substrate CtsR to the ClpCP machinery only when phosphorylated (54). According to our genetic data, either ReoM or ReoY could act as this adaptor, leaving a subsidiary function for the other respective protein. Alternatively, both proteins

bioRxiv preprint doi: https://doi.org/10.1101/2019.12.16.877605; this version posted December 17, 2019. The copyright holder for this preprint (which was not certified by peer review) is the author/funder. All rights reserved. No reuse allowed without permission.

could work in tandem, where each of them is equally needed for ClpCP-dependent MurA degradation since the phenotypes of *reoM* and *reoY* mutants were identical with respect to MurA stability. However, overexpression or deletion of *reoM* altered the phenotype of the Δ*gpsB* mutant, but that of *reoY* was without phenotype (Fig. S1, Fig. S2). ReoY, restricted to the *Bacilli*, also showed a narrower phylogenetic distribution than ReoM, which is found across different Firmicutes (Fig. 5B). Thus, it seems that ReoM might have a more generalized role, whereas ReoY could play a subordinate function in control of MurA degradation by ClpCP. The role of the MurA homologue MurZ in this process is entirely unclear, but our genetic data now place it downstream of ReoM (Fig. 8). Furthermore, arginine phosphorylation targets proteins to ClpCP for degradation (55). *L. monocytogenes* MurA contains 17 arginines and MurAA of *B. subtilis* has been found in complex with the protein arginine phosphatase YwlE (56). The possibility that MurA proteins could also require arginine phosphorylation to be accepted as a substrate by ClpCP offers additional control possibilities for ReoM/ReoY/MurZ to modulate MurA levels.

A screen for *gpsB* suppressors in *S. pneumoniae* D39 and Rx1 strains did not yield *reoM* mutations (and these strains do not contain *reoY*, consistent with a subordinate function for this gene), but instead suppressor mutations were found that affect *phpP*, which encodes a Ser/Thr protein phosphatase that acts in concert with StkP, the PASTA-eSTK of this organism (57, 58). Absence or inactivation of PhpP triggered an increase in StkP-dependent protein phosphorylation levels in the pneumococcus (57, 59). It is tempting to speculate that loss of PhpP activity in this suppressor also triggers P-ReoM formation that, according to our model, would help to stabilize MurA and thus suppress the Δ*gpsB* phenotype. Interestingly, another *S. pneumoniae gpsB* suppressor was identified that carries a duplication of a ~150 kb genomic fragment (57), a region that includes the open reading frame for MurA. Suppression of the *gpsB* phenotype in this instance could also work via MurA accumulation, but this time due to a gene dosage effect.

bioRxiv preprint doi: https://doi.org/10.1101/2019.12.16.877605; this version posted December 17, 2019. The copyright holder for this preprint (which was not certified by peer review) is the author/funder. All rights reserved. No reuse allowed without permission.

411 It is becoming increasingly evident that control of PG biosynthesis in response to cell wall
412 derived signals, via PASTA-eSTKs, is a regulatory capacity common to Firmicutes and
413 Actinobacteria. CwlM is the critical kinase substrate in the Actinobacterium *M. tuberculosis* that,
414 when phosphorylated by PknB, binds to and activates MurA (23). Full-length homologues of
415 CwlM are not present in *L. monocytogenes* or *B. subtilis* and instead these bacteria adjust their
416 MurA levels by controlling MurA turnover in response to PrkA-dependent phosphorylation of
417 ReoM. Consequently, both mechanisms activate PG biosynthesis in a PrkA-dependent manner
418 either by activation or stabilization of MurA. Presumably *B. subtilis*, and other endospore
419 forming bacteria, must re-start PG biosynthesis at the onset of germination in a similar way.
420 Germination of *B. subtilis* spores can be triggered by muropeptides in a manner that depends
421 upon PrkC (49), the PASTA-eSTK of *B. subtilis* (60). Even though *Bs*PrkC phosphorylates
422 multiple substrates (61), whose individual contribution to germination is not known precisely,
423 phosphorylation of ReoM (*aka* YrzL) could be required to restart PG biosynthesis in germinating
424 *B. subtilis* cells by stabilizing MurAA. Moreover, an *E. faecalis* mutant lacking the PASTA-
425 eSTK IreK was more susceptible to the third-generation cephalosporin ceftriaxone but
426 overexpression of *Ef*MurAA overcame this defect (62). This implies the possibility that
427 unphosphorylated IreB might stimulate MurAA proteolysis in *E. faecalis* as well. Taken together
428 it seems that observations made in different Firmicutes are in good agreement with the
429 PrkA→ReoM/ReoY→ClpC→MurA signaling sequence that we propose. The open questions
430 that remain on the molecular mechanism of ClpCP control by ReoM and ReoY will be addressed
431 by future experiments.
432

bioRxiv preprint doi: https://doi.org/10.1101/2019.12.16.877605; this version posted December 17, 2019. The copyright holder for this preprint (which was not certified by peer review) is the author/funder. All rights reserved. No reuse allowed without permission.

METHODS

Bacterial strains and growth conditions

Table 1 lists all strains used in this study. Strains of *L. monocytogenes* were cultivated in BHI broth or on BHI agar plates. *B. subtilis* strains were grown in LB broth at 37°C. Antibiotics and supplements were added when required at the following concentrations: erythromycin (5 µg/ml), kanamycin (50 µg/ml), X-Gal (100 µg/ml) and IPTG (as indicated). *Escherichia coli* TOP10 was used as host for all cloning procedures (63).

General methods, manipulation of DNA and oligonucleotide primers

Standard methods were used for transformation of *E. coli* and isolation of plasmid DNA (63). Transformation of *L. monocytogenes* was carried out as described by others (64). Restriction and ligation of DNA was performed according to the manufacturer´s instructions. All primer sequences are listed in Table 2.

Construction of plasmids for recombinant protein expression

The plasmids for expressing recombinant versions of ReoM, PrkA-KD and PrkP were prepared by first amplifying the corresponding genes (*reoM*, *lmo1820* and *lmo1821*) from *L. monocytogenes* EGD-e genomic DNA using primer pairs Lmo1503F/Lmo1503R, PrkAF/PrkAR, and PrkPF/PrkPR, respectively. The PCR products were individually ligated between the *Nco*I and *Xho*I sites of pETM11 (65). All mutagenesis was carried out using the Quikchange protocol and the correct sequence of each plasmid and mutant constructed was verified by Sanger DNA sequencing (Eurofins Genomics).

bioRxiv preprint doi: https://doi.org/10.1101/2019.12.16.877605; this version posted December 17, 2019. The copyright holder for this preprint (which was not certified by peer review) is the author/funder. All rights reserved. No reuse allowed without permission.

Construction of plasmids for generation of *L. monocytogenes* strains

Plasmid pJR65 was constructed for the inducible expression of *reoM*. To this end, the *reoM* open reading frame was amplified by PCR using the oligonucleotides JR169/JR170 and cloned into pIMK3 using NcoI/SalI. The T7A mutation were introduced into *reoM* of plasmid pJR65 by quickchange mutagenesis using the primer pair SW77/SW78, yielding pSW29. The R57A, R62A R66A and R70A, mutations were introduced into pJR65 in the same way, but using primer pairs SW144/SW145, SW146/SW147, SW136/SW137 and SW138/SW139, respectively.

Plasmid pJR70 was constructed for inducible *reoY* expression. For this purpose, *reoY* was amplified using the primer pair JR163/JR164 and cloned into pIMK3 using NcoI/SalI.

Plasmid pSW38, for IPTG-inducible *prkA* expression, was constructed by amplification of *prkA* using the oligonucleotides SW112/SW113 and the subsequent cloning of the generated fragment into pIMK3 using BamHI/SalI. Plasmid pSW39, for IPTG-controlled expression of *prkP*, was constructed analogously, but using the oligonucleotides SW110/SW111 as the primers.

For construction of plasmid pJR83, facilitating deletion of *reoY*, fragments encompassing ~800 bp up- and down-stream of *reoY* were amplified by PCR with the primer pairs JR197/JR198 and JR199/JR200. Both fragments were spliced together by splicing by overlapping extension (SOE) PCR and cloned into pMAD using BamHI/EcoRI.

Plasmid pJR126 was generated for deletion of *reoM*. Fragments up- and down-stream of *reoM* were PCR amplified using the primers JR264/JR265 and JR266/JR267. Both fragments were cut with BamHI, fused together by ligation and the desired fragment was amplified from the ligation mixture by PCR using the primers JR264/JR267 and then cloned into pMAD using BglII/SalI.

Plasmid pSW36 was constructed to delete the *prkA* gene. Fragments up- and down-stream of *prkA* were amplified in separate PCRs using the primer pairs SHW819/SHW821 and SHW820/SHW822. Both fragments were fused together by SOE-PCR and inserted into pMAD

bioRxiv preprint doi: https://doi.org/10.1101/2019.12.16.877605; this version posted December 17, 2019. The copyright holder for this preprint (which was not certified by peer review) is the author/funder. All rights reserved. No reuse allowed without permission.

by restriction free cloning (66). Plasmid pSW37, facilitating deletion of *prkP*, was constructed in a similar manner. Up- and down-stream fragments of *prkP* were amplified using the primer pairs SHW815/SHW817 and SHW816/SHW818 and fused together by SOE-PCR. The resulting fragment was inserted into pMAD by restriction free cloning.

Derivatives of pIMK3 were introduced into *L. monocytogenes* strains by electroporation and clones were selected on BHI agar plates containing kanamycin. Plasmid insertion at the *attB* site of the $tRNA^{Arg}$ locus was verified by PCR. Plasmid derivatives of pMAD were transformed into the respective *L. monocytogenes* recipient strains and genes were deleted as described elsewhere (67). All gene deletions were confirmed by PCR.

Genome sequencing

A total of 1 ng of genomic DNA was used for library generation by the Nextera XT DNA Library Prep Kit according to the manufacturer's recommendations (Illumina). Sequencing was carried out on a MiSeq benchtop sequencer and performed in paired-end modes (2 x 300 bp) using a MiSeq Reagent Kit v3 cartridge (600-cycle kit). Sequencing reads were mapped to the reference genome *L. monocytogenes* EGD-e (NC_003210.1) (68) by utilizing the Geneious software (Biomatters Ltd.). Variants, representing putative suppressor mutations, were identified using the Geneious SNP finder tool. Genome sequences of *shg8*, *shg10*, *shg12* and LMSW76 were deposited at ENA under study number PRJEB35110 and sample accession numbers ERS3927571 (SAMEA6127277), ERS3927572 (SAMEA6127278), ERS3927573 (SAMEA6127279), and ERS3967687 (SAMEA6167687) respectively.

bioRxiv preprint doi: https://doi.org/10.1101/2019.12.16.877605; this version posted December 17, 2019. The copyright holder for this preprint (which was not certified by peer review) is the author/funder. All rights reserved. No reuse allowed without permission.

503 **Isolation of cellular proteins and Western blotting**

504 Cells were harvested by centrifugation (13,000 rpm, 1 min in a table-top centrifuge), washed with
505 ZAP buffer (10 mM Tris.HCl pH7.5, 200 mM NaCl), resuspended in 1 ml ZAP buffer also
506 containing 1 mM PMSF and disrupted by sonication. Centrifugation was used to remove cellular
507 debris and the supernatant was used as total cellular protein extract. Sample aliquots were
508 separated by standard SDS polyacrylamide gel electrophoresis. Gels were transferred onto
509 positively charged polyvinylidene fluoride membranes by semi-dry transfer. ClpC, GlmS, IlvB
510 and MurA were immune-stained using a polyclonal rabbit antiserum recognizing *B. subtilis* ClpC
511 (28), DivIVA (69), GlmS, IlvB (42) and MurAA (26) as the primary antibody and an anti-rabbit
512 immunoglobulin G conjugated to horseradish peroxidase as the secondary one. The ECL
513 chemiluminescence detection system (Thermo Scientific) was used for detection of the
514 peroxidase conjugates on the PVDF membrane in a chemiluminescence imager (Vilber Lourmat).
515 For depletion of PrkA, PrkA depletion strains were grown overnight in the presence of 1 mM
516 IPTG and then again inoculated in BHI broth containing 1 mM IPTG to an OD_{600}=0.05 and
517 grown for 3 h at 37°C. Subsequently, cells were centrifuged, washed and reinoculated in BHI
518 broth without IPTG at the same OD_{600} as before centrifugation. Finally, cells were harvested after
519 3.5 more hours of growth at 37°C and cellular proteins were isolated.
520
521 **Microscopy**
522 Cytoplasmic membranes of exponentially growing bacteria were stained through addition of 1 µl
523 of nile red solution (100 µg ml^{-1} in DMSO) to 100 µl of culture. Images were taken with a Nikon
524 Eclipse Ti microscope coupled to a Nikon DS-MBWc CCD camera and processed using the NIS
525 elements AR software package (Nikon) or ImageJ. Scanning electron microscopy was performed
526 essentially as described earlier (70).

bioRxiv preprint doi: https://doi.org/10.1101/2019.12.16.877605; this version posted December 17, 2019. The copyright holder for this preprint (which was not certified by peer review) is the author/funder. All rights reserved. No reuse allowed without permission.

527 **Recombinant protein purification**

528 All proteins were expressed in *E. coli* BL21 (DE3) cells. Cell cultures were grown at 37°C in LB
529 liquid media supplemented with 50 µg mL^{-1} kanamycin to an OD_{600} 0.6-0.8 before expression
530 was induced by the addition of IPTG to a final concentration of 0.4 mM IPTG. The cultures were
531 incubated at 20°C overnight before the cells from 2 L of cell culture were harvested by
532 centrifugation at 3500 x g for 30 minutes. The cell pellets were resuspended in 70 mL of buffer A
533 (50 mM Tris.HCl, pH 8, 300 mM NaCl, 10 mM imidazole) with 500 Kunitz units of DNase I and
534 1 mL Roche complete protease inhibitor cocktail at 25x working concentration. The cells were
535 lysed by sonication, centrifuged at 19000 x g for 20 minutes and the supernatant was filtered
536 using a 0.45 µm filter. The clarified cell lysate was loaded onto a 5 mL Ni-NTA superflow
537 cartridge (Qiagen), washed with buffer A, and bound proteins were eluted with 50 mM Tris.HCl,
538 pH 8, 300 mM NaCl, 250 mM imidazole. The His_6-tag of PrkA-KD was cleaved with His-tagged
539 TEV protease (1 mg TEV for 20 mg of protein) at 4 °C during an overnight dialysis against a
540 buffer of 50 mM Tris.HCl, pH 8, 300 mM NaCl, 10 mM imidazole, 1 mM DTT; TEV cleavage
541 of ReoM was conducted as above except the dialysis was carried out at 20 °C. The proteolysis
542 reaction products were then passed over a 5 mL Ni-NTA superflow cartridge (Qiagen) to remove
543 TEV and uncleaved protein. The proteins that did not bind to the Ni-NTA column were
544 concentrated and loaded onto either a Superdex 75 XK16/60 (GE Healthcare) (ReoM) or a
545 Superdex 200 XK16/60 (GE Healthcare) (PrkA-KD and PrkP) equilibrated with 10 mM Na-
546 HEPES, pH 8, 100 mM NaCl for size exclusion chromatography. Fractions from the gel filtration
547 were analysed for purity by SDS-PAGE, concentrated to 20-40 mg mL^{-1}, and small aliquots were
548 snap-frozen in liquid nitrogen for storage at -80°C.
549

bioRxiv preprint doi: https://doi.org/10.1101/2019.12.16.877605; this version posted December 17, 2019. The copyright holder for this preprint (which was not certified by peer review) is the author/funder. All rights reserved. No reuse allowed without permission.

550 **X-ray crystallography and ReoM structure determination**

551 For ReoM, 23 mg mL^{-1} of protein in 10 mM Na-HEPES pH 8, 100 mM NaCl was subjected to
552 crystallisation by sparse matrix screening using a panel of commercial crystallisation screens. 100
553 and 200 nL drops of protein and 100 nL of screen solution were dispensed into 96 well MRC
554 crystallization plates (Molecular Dimensions) by a Mosquito (TTP Labtech) liquid handling robot
555 and the crystallisation plates were stored at a constant temperature of 20°C. The crystals that
556 grew and were subsequently used for diffraction experiments were formed in 0.1 M
557 phosphate/citrate pH 4.2, 0.2 M lithium sulfate, 20 % w/v PEG 1000 from the JCSG + screen and
558 were mounted onto rayon loops directly from the crystallization drops and cryo-cooled in liquid
559 nitrogen.
560 Diffraction data were collected on beamline I03 at the Diamond Light Source (DLS) synchrotron.
561 Diffraction images were integrated in MOSFLM (71) and scaled and merged with AIMLESS
562 (72). The initial model was generated by molecular replacement in PHASER (73) using the
563 dimeric, 20-conformer ensemble model (PDBid 5US5) of IreB solved by nuclear magnetic
564 resonance (46) as a search model. The final model was produced by iterative cycles of model
565 building in COOT (74) with refinement in REFMAC (75) until convergence. The diffraction data
566 collection and model refinement statistics are summarised in Table 3.
567

568 **Protein phosphorylation and dephosphorylation**

569 The effect of phosphorylation and dephosphorylation on ReoM and PrkA-KD proteins was
570 analysed by 20% non-denaturing PAGE. Phosphorylation reactions consisted of 18.5 µM ReoM,
571 3.7 µM PrkA-KD, 5 mM ATP and 5 mM $MgCl_2$, diluted in 10 mM HEPES.HCl pH 8.0 and 100
572 mM NaCl. Dephosphorylation reactions consisted of 37 µM P-ReoM, 3.7 µM PrkA-KD, 18.5
573 µM PrkP and 1 mM $MnCl_2$, diluted in 10 mM HEPES.HCl pH 8.0 and 100 mM NaCl. In each

bioRxiv preprint doi: https://doi.org/10.1101/2019.12.16.877605; this version posted December 17, 2019. The copyright holder for this preprint (which was not certified by peer review) is the author/funder. All rights reserved. No reuse allowed without permission.

574 case controls were loaded at the same concentrations. The reactions were incubated at 37 °C for
575 20 minutes prior to electrophoresis at 200 V for 2.5 hours on ice.
576
577 **Isolation of phosphorylated ReoM**
578 Phosphorylation reactions consisted of 37 µM ReoM, 3.7 µM PrkA-KD, 5 mM ATP and 5 mM
579 $MgCl_2$, diluted in 10 mM HEPES.HCl pH 8.0 and 100 mM NaCl, to a total volume of 5 mL. The
580 protein mix was loaded onto a PD 10 desalting column to remove excess ATP and protein
581 fractions were loaded onto a MonoQ 5/50 GL column. Buffer A consisted of 10 mM HEPES.HCl
582 pH 8.0 and 100 mM NaCl and buffer B was 10 mM HEPES.HCl pH 8.0 and 1M NaCl. Bound
583 proteins were eluted over 25 mL with a 15-35% gradient of buffer B.
584
585 **Liquid Chromatography-Mass Spectrometry**
586 All liquid chromatography-mass spectrometry (LC-MS) analyses were performed using an
587 Agilent 6530 Q-TOF instrument with electrospray ionisation (ESI) in positive ion mode, coupled
588 to an Agilent 1260 Infinity II LC system, utilizing mobile phase of 0.1% (v/v) formic acid in LC-
589 MS grade water (A) and acetonitrile (B). Prior to peptide mapping, 10 µL of purified proteins (~1
590 mg/ml) were digested using Smart Digest Soluble Trypsin Kit (Thermo Fisher Scientific)
591 according to the manufacturer's guidelines. Tryptic peptides and intact protein samples were
592 extracted using HyperSep Spin Tip SPE C18 and C8 tips, respectively (ThermoFisher Scientific)
593 before analysis. For phosphosite analysis, 10 µL of digest was injected onto an Acclaim RSLC
594 120 C18 column (Thermo Fisher Scientific, 2.1 x 100mm, 2.2 µm, 120 Å) for reversed phase
595 separation at 60°C and 0.4 ml/min, over a linear gradient of 5-40% B over 25 min, 40-90% B
596 over 8 min followed by equilibration at 5% B for 7 min. ESI source conditions were nebuliser
597 pressure of 45 psig, drying gas flow of 5 L/min and gas temperature of 325°C. Sheath gas

bioRxiv preprint doi: https://doi.org/10.1101/2019.12.16.877605; this version posted December 17, 2019. The copyright holder for this preprint (which was not certified by peer review) is the author/funder. All rights reserved. No reuse allowed without permission.

598 temperature of 275°C and gas flow of 12 L/min, capillary voltage of 4000V and nozzle voltage of
599 300V were also applied. Mass spectra were acquired using MassHunter Acquisition software
600 (version B.08.00) over the 100-3000 m/z range, at a rate of 5 spectra/s and 200 ms/spectrum,
601 using standard mass range mode (3200 m/z) with extended dynamic range (2 GHz) and collection
602 of both centroid and profile data. MS/MS fragmentation spectra were acquired over the 100-3000
603 m/z range, at a rate of 3 spectra/s and 333.3 ms/spectrum. For intact protein analysis,10 µL of
604 desalted protein (~1 mg/ml) was injected onto a Zorbax 300Å Stable Bond C8 column (Agilent
605 Technologies, 4.6 x 50 mm, 3.5 µM) for reversed phase separation at 60°C and 0.4 mL/min, over
606 a linear gradient of 15-75% B over 14 min, 75-100% B over 11 min followed by post-run
607 equilibration at 15% B for 10 min. ESI source conditions were nebuliser pressure of 45 psig,
608 drying gas flow of 5 L/min and source gas temperature of 325°C were applied. Sheath gas
609 temperature of 400°C and gas flow of 11 L/min, capillary voltage of 3500V and nozzle voltage of
610 2000V were also used. Mass spectra were acquired using MassHunter Acquisition software
611 (version B.08.00) over a mass range of 100-3000 m/z, at a rate of 1 spectra/s and 1000
612 ms/spectrum in extended mass range (20000 m/z) at 1 GHz. Acquired MS and MS/MS spectra
613 were analysed using Agilent MassHunter BioConfirm software (version B.10.00) for
614 identification of phosphorylated residues and subsequent intact mass determination with
615 processing of raw data using maximum entropy deconvolution.
616
617 **Analytical size exclusion chromatography**
618 Purified ReoM and P-ReoM proteins were run individually on a Superdex 200 Increase 10/300
619 GL column. 100 µl samples at 1.5 mg/mL were injected onto a column equilibrated in 10 mM
620 HEPES.HCl pH 8.0 and 100 mM NaCl, with a flow of 0.75 mL/min.
621

bioRxiv preprint doi: https://doi.org/10.1101/2019.12.16.877605; this version posted December 17, 2019. The copyright holder for this preprint (which was not certified by peer review) is the author/funder. All rights reserved. No reuse allowed without permission.

ACKNOWLEDGEMENTS

This work was funded by DFG grants HA 6830/1-1 and HA 6830/1-2 and a grant of the Fonds der Chemischen Industrie to SH. ZR is funded by a UK BBSRC DTP studentship to RJL (BB/M011186/1). We acknowledge Diamond Light Source for time on beamline I03 under proposal MX-18598 and Dr. Arnaud Basle for help with X-ray data collection. We thank Ulrich Nübel (Braunschweig) and Janina Döhling for help with some experiments and Petra Kaiser for technical assistance. We would like to thank the National BioResource Project (NIG, Japan): *B. subtilis* for sharing *B. subtilis* mutant strains. The co-ordinates and structure factors for the crystal structure of ReoM have been deposited at PDBe with accession code 6TIF.

.

AUTHOR CONTRIBUTIONS

SW, ZJR, JR, CEJ, LM, RJL and SH designed the experiments. SW, ZJR, JR, CEJ and LM performed the experimental work. SW, ZJR, JR, CEJ, LM, RJL and SH interpreted the data. RJL and SH wrote the manuscript.

COMPETING INTERESTS STATEMENT

All authors declare that NO conflicting interests exist.

bioRxiv preprint doi: https://doi.org/10.1101/2019.12.16.877605; this version posted December 17, 2019. The copyright holder for this preprint (which was not certified by peer review) is the author/funder. All rights reserved. No reuse allowed without permission.

REFERENCES

1. Vollmer W, Blanot D, & de Pedro MA (2008) Peptidoglycan structure and architecture. *FEMS Microbiol Rev* 32(2):149-167.
2. Typas A, Banzhaf M, Gross CA, & Vollmer W (2012) From the regulation of peptidoglycan synthesis to bacterial growth and morphology. *Nat Rev Microbiol* 10(2):123-136.
3. Ruiz N (2008) Bioinformatics identification of MurJ (MviN) as the peptidoglycan lipid II flippase in *Escherichia coli*. *Proc Natl Acad Sci U S A* 105(40):15553-15557.
4. Sham LT*, et al.* (2014) Bacterial cell wall. MurJ is the flippase of lipid-linked precursors for peptidoglycan biogenesis. *Science* 345(6193):220-222.
5. Meeske AJ*, et al.* (2015) MurJ and a novel lipid II flippase are required for cell wall biogenesis in *Bacillus subtilis*. *Proc Natl Acad Sci U S A* 112(20):6437-6442.
6. Sauvage E, Kerff F, Terrak M, Ayala JA, & Charlier P (2008) The penicillin-binding proteins: structure and role in peptidoglycan biosynthesis. *FEMS Microbiol Rev* 32(2):234-258.
7. Meeske AJ*, et al.* (2016) SEDS proteins are a widespread family of bacterial cell wall polymerases. *Nature* 537(7622):634-638.
8. Emami K*, et al.* (2017) RodA as the missing glycosyltransferase in *Bacillus subtilis* and antibiotic discovery for the peptidoglycan polymerase pathway. *Nat Microbiol* 2:16253.
9. Taguchi A*, et al.* (2019) FtsW is a peptidoglycan polymerase that is functional only in complex with its cognate penicillin-binding protein. *Nat Microbiol*.
10. Vollmer W, Joris B, Charlier P, & Foster S (2008) Bacterial peptidoglycan (murein) hydrolases. *FEMS Microbiol Rev* 32(2):259-286.
11. Uehara T & Bernhardt TG (2011) More than just lysins: peptidoglycan hydrolases tailor the cell wall. *Curr Opin Microbiol* 14(6):698-703.
12. Moynihan PJ, Sychantha D, & Clarke AJ (2014) Chemical biology of peptidoglycan acetylation and deacetylation. *Bioorg Chem* 54:44-50.
13. Booth S & Lewis RJ (2019) Structural basis for the coordination of cell division with the synthesis of the bacterial cell envelope. *Protein science : a publication of the Protein Society*.
14. Dworkin J (2015) Ser/Thr phosphorylation as a regulatory mechanism in bacteria. *Curr Opin Microbiol* 24:47-52.
15. Manuse S, Fleurie A, Zucchini L, Lesterlin C, & Grangeasse C (2016) Role of eukaryotic-like serine/threonine kinases in bacterial cell division and morphogenesis. *FEMS Microbiol Rev* 40(1):41-56.
16. Egan AJ, Cleverley RM, Peters K, Lewis RJ, & Vollmer W (2017) Regulation of bacterial cell wall growth. *FEBS J* 284(6):851-867.
17. Mir M*, et al.* (2011) The extracytoplasmic domain of the *Mycobacterium tuberculosis* Ser/Thr kinase PknB binds specific muropeptides and is required for PknB localization. *PLoS Pathog* 7(7):e1002182.
18. Hardt P*, et al.* (2017) The cell wall precursor lipid II acts as a molecular signal for the Ser/Thr kinase PknB of *Staphylococcus aureus*. *Int J Med Microbiol* 307(1):1-10.
19. Parikh A, Verma SK, Khan S, Prakash B, & Nandicoori VK (2009) PknB-mediated phosphorylation of a novel substrate, N-acetylglucosamine-1-phosphate uridyltransferase, modulates its acetyltransferase activity. *J Mol Biol* 386(2):451-464.
20. Gee CL*, et al.* (2012) A phosphorylated pseudokinase complex controls cell wall synthesis in mycobacteria. *Sci Signal* 5(208):ra7.
21. Kieser KJ*, et al.* (2015) Phosphorylation of the Peptidoglycan Synthase PonA1 Governs the Rate of Polar Elongation in Mycobacteria. *PLoS Pathog* 11(6):e1005010.
22. Deng LL*, et al.* (2005) Identification of a novel peptidoglycan hydrolase CwlM in *Mycobacterium tuberculosis*. *Biochimica et biophysica acta* 1747(1):57-66.

bioRxiv preprint doi: https://doi.org/10.1101/2019.12.16.877605; this version posted December 17, 2019. The copyright holder for this preprint (which was not certified by peer review) is the author/funder. All rights reserved. No reuse allowed without permission.

23. Boutte CC*, et al.* (2016) A cytoplasmic peptidoglycan amidase homologue controls mycobacterial cell wall synthesis. *eLife* 5.
24. Turapov O*, et al.* (2018) Two Faces of CwlM, an Essential PknB Substrate, in *Mycobacterium tuberculosis*. *Cell reports* 25(1):57-67 e55.
25. Brown ED, Vivas EI, Walsh CT, & Kolter R (1995) MurA (MurZ), the enzyme that catalyzes the first committed step in peptidoglycan biosynthesis, is essential in *Escherichia coli*. *J Bacteriol* 177(14):4194-4197.
26. Kock H, Gerth U, & Hecker M (2004) MurAA, catalysing the first committed step in peptidoglycan biosynthesis, is a target of Clp-dependent proteolysis in *Bacillus subtilis*. *Mol Microbiol* 51(4):1087-1102.
27. Griffin JE*, et al.* (2011) High-resolution phenotypic profiling defines genes essential for mycobacterial growth and cholesterol catabolism. *PLoS Pathog* 7(9):e1002251.
28. Rismondo J, Bender JK, & Halbedel S (2017) Suppressor mutations linking *gpsB* with the first committed step of peptidoglycan biosynthesis in *Listeria monocytogenes*. *J Bacteriol* 199(1).
29. Pensinger DA*, et al.* (2016) The *Listeria monocytogenes* PASTA Kinase PrkA and its substrate YvcK are required for cell wall homeostasis, metabolism, and virulence. *PLoS Pathog* 12(11):e1006001.
30. Macek B*, et al.* (2007) The serine/threonine/tyrosine phosphoproteome of the model bacterium *Bacillus subtilis*. *Molecular & cellular proteomics : MCP* 6(4):697-707.
31. Pompeo F, Foulquier E, Serrano B, Grangeasse C, & Galinier A (2015) Phosphorylation of the cell division protein GpsB regulates PrkC kinase activity through a negative feedback loop in *Bacillus subtilis*. *Mol Microbiol* 97(1):139-150.
32. Rismondo J*, et al.* (2016) Structure of the bacterial cell division determinant GpsB and its interaction with penicillin-binding proteins. *Mol Microbiol* 99(5):978-998.
33. Cleverley RM*, et al.* (2016) Subunit arrangement in GpsB, a regulator of cell wall biosynthesis. *Microbial drug resistance* 22(6):446-460.
34. Cleverley RM*, et al.* (2019) The cell cycle regulator GpsB functions as cytosolic adaptor for multiple cell wall enzymes. *Nature communications* 10(1):261.
35. Halbedel S & Lewis RJ (2019) Structural basis for interaction of DivIVA/GpsB proteins with their ligands. *Mol Microbiol* 111(6):1404-1415.
36. Moliere N & Turgay K (2009) Chaperone-protease systems in regulation and protein quality control in *Bacillus subtilis*. *Res Microbiol* 160(9):637-644.
37. Hall CL, Tschannen M, Worthey EA, & Kristich CJ (2013) IreB, a Ser/Thr kinase substrate, influences antimicrobial resistance in *Enterococcus faecalis*. *Antimicrob Agents Chemother* 57(12):6179-6186.
38. Nicolas P*, et al.* (2012) Condition-dependent transcriptome reveals high-level regulatory architecture in *Bacillus subtilis*. *Science* 335(6072):1103-1106.
39. Chopin A, Biaudet V, & Ehrlich SD (1998) Analysis of the *Bacillus subtilis* genome sequence reveals nine new T-box leaders. *Mol Microbiol* 29(2):662-664.
40. Kurata T*, et al.* (2015) Novel essential gene Involved in 16S rRNA processing in *Escherichia coli*. *J Mol Biol* 427(4):955-965.
41. Tam le T*, et al.* (2006) Proteome signatures for stress and starvation in *Bacillus subtilis* as revealed by a 2-D gel image color coding approach. *Proteomics* 6(16):4565-4585.
42. Gerth U*, et al.* (2008) Clp-dependent proteolysis down-regulates central metabolic pathways in glucose-starved *Bacillus subtilis*. *J Bacteriol* 190(1):321-331.
43. Kennelly PJ (2001) Protein phosphatases--a phylogenetic perspective. *Chemical reviews* 101(8):2291-2312.
44. Madec E*, et al.* (2003) Mass spectrometry and site-directed mutagenesis identify several autophosphorylated residues required for the activity of PrkC, a Ser/Thr kinase from *Bacillus subtilis*. *J Mol Biol* 330(3):459-472.

bioRxiv preprint doi: https://doi.org/10.1101/2019.12.16.877605; this version posted December 17, 2019. The copyright holder for this preprint (which was not certified by peer review) is the author/funder. All rights reserved. No reuse allowed without permission.

45. Kristich CJ, Little JL, Hall CL, & Hoff JS (2011) Reciprocal regulation of cephalosporin resistance in *Enterococcus faecalis*. *mBio* 2(6):e00199-00111.
46. Hall CL*, et al.* (2017) Structure and Dimerization of IreB, a Negative Regulator of Cephalosporin Resistance in *Enterococcus faecalis*. *J Mol Biol* 429(15):2324-2336.
47. Johnson LN & Lewis RJ (2001) Structural basis for control by phosphorylation. *Chemical reviews* 101(8):2209-2242.
48. Rakette S, Donat S, Ohlsen K, & Stehle T (2012) Structural analysis of *Staphylococcus aureus* serine/threonine kinase PknB. *PLoS One* 7(6):e39136.
49. Shah IM, Laaberki MH, Popham DL, & Dworkin J (2008) A eukaryotic-like Ser/Thr kinase signals bacteria to exit dormancy in response to peptidoglycan fragments. *Cell* 135(3):486-496.
50. Irazoki O, Hernandez SB, & Cava F (2019) Peptidoglycan Muropeptides: Release, Perception, and Functions as Signaling Molecules. *Frontiers in microbiology* 10:500.
51. Kohlrausch U & Höltje JV (1991) Analysis of murein and murein precursors during antibiotic-induced lysis of *Escherichia coli*. *J Bacteriol* 173(11):3425-3431.
52. Kirstein J, Molière N, Dougan DA, & Turgay K (2009) Adapting the machine: adaptor proteins for Hsp100/Clp and AAA+ proteases. *Nature Reviews Microbiology* 7:589.
53. Mulvenna N*, et al.* (2019) Xenogeneic modulation of the ClpCP protease of *Bacillus subtilis* by a phage-encoded adaptor-like protein. *Journal of Biological Chemistry*.
54. Kirstein J, Dougan DA, Gerth U, Hecker M, & Turgay K (2007) The tyrosine kinase McsB is a regulated adaptor protein for ClpCP. *The EMBO Journal* 26(8):2061-2070.
55. Trentini DB*, et al.* (2016) Arginine phosphorylation marks proteins for degradation by a Clp protease. *Nature* 539(7627):48-53.
56. Elsholz AK*, et al.* (2012) Global impact of protein arginine phosphorylation on the physiology of *Bacillus subtilis*. *Proc Natl Acad Sci U S A* 109(19):7451-7456.
57. Rued BE*, et al.* (2017) Suppression and synthetic-lethal genetic relationships of DeltagpsB mutations indicate that GpsB mediates protein phosphorylation and penicillin-binding protein interactions in *Streptococcus pneumoniae* D39. *Mol Microbiol* 103(6):931-957.
58. Lewis RJ (2017) The GpsB files: the truth is out there. *Mol Microbiol* 103(6):913-918.
59. Ulrych A*, et al.* (2016) Characterization of pneumococcal Ser/Thr protein phosphatase *phpP* mutant and identification of a novel PhpP substrate, putative RNA binding protein Jag. *BMC Microbiology* 16(1):247.
60. Madec E, Laszkiewicz A, Iwanicki A, Obuchowski M, & Seror S (2002) Characterization of a membrane-linked Ser/Thr protein kinase in *Bacillus subtilis*, implicated in developmental processes. *Mol Microbiol* 46(2):571-586.
61. Ravikumar V*, et al.* (2014) Quantitative phosphoproteome analysis of *Bacillus subtilis* reveals novel substrates of the kinase PrkC and phosphatase PrpC. *Molecular & cellular proteomics : MCP* 13(8):1965-1978.
62. Vesic D & Kristich CJ (2012) MurAA is required for intrinsic cephalosporin resistance of *Enterococcus faecalis*. *Antimicrob Agents Chemother* 56(5):2443-2451.
63. Sambrook J, Fritsch EF, & Maniatis T (1989) *Molecular cloning : a laboratory manual* (Cold Spring Harbor Laboratory Press, Cold Spring Harbor, N.Y.) 2nd Ed p 3 v.
64. Monk IR, Gahan CG, & Hill C (2008) Tools for functional postgenomic analysis of *Listeria monocytogenes*. *Appl Environ Microbiol* 74(13):3921-3934.
65. Peränen J, Rikkonen M, Hyvonen M, & Kaariainen L (1996) T7 vectors with modified T7lac promoter for expression of proteins in *Escherichia coli*. *Anal Biochem* 236(2):371-373.
66. van den Ent F & Löwe J (2006) RF cloning: a restriction-free method for inserting target genes into plasmids. *J Biochem Biophys Methods* 67(1):67-74.

bioRxiv preprint doi: https://doi.org/10.1101/2019.12.16.877605; this version posted December 17, 2019. The copyright holder for this preprint (which was not certified by peer review) is the author/funder. All rights reserved. No reuse allowed without permission.

67. Arnaud M, Chastanet A, & Debarbouille M (2004) New vector for efficient allelic replacement in naturally nontransformable, low-GC-content, gram-positive bacteria. *Appl Environ Microbiol* 70(11):6887-6891.
68. Glaser P*, et al.* (2001) Comparative genomics of *Listeria* species. *Science* 294(5543):849-852.
69. Marston AL, Thomaides HB, Edwards DH, Sharpe ME, & Errington J (1998) Polar localization of the MinD protein of *Bacillus subtilis* and its role in selection of the mid-cell division site. *Genes Dev* 12(21):3419-3430.
70. Rismondo J*, et al.* (2015) Discrete and overlapping functions of peptidoglycan synthases in growth, cell division and virulence of *Listeria monocytogenes*. *Mol Microbiol* 95(2):332-351.
71. Battye TG, Kontogiannis L, Johnson O, Powell HR, & Leslie AG (2011) iMOSFLM: a new graphical interface for diffraction-image processing with MOSFLM. *Acta crystallographica. Section D, Biological crystallography* 67(Pt 4):271-281.
72. Evans PR & Murshudov GN (2013) How good are my data and what is the resolution? *Acta crystallographica. Section D, Biological crystallography* 69(Pt 7):1204-1214.
73. McCoy AJ*, et al.* (2007) Phaser crystallographic software. *Journal of applied crystallography* 40(Pt 4):658-674.
74. Emsley P, Lohkamp B, Scott WG, & Cowtan K (2010) Features and development of Coot. *Acta crystallographica. Section D, Biological crystallography* 66(Pt 4):486-501.
75. Murshudov GN, Vagin AA, & Dodson EJ (1997) Refinement of macromolecular structures by the maximum-likelihood method. *Acta crystallographica. Section D, Biological crystallography* 53(Pt 3):240-255.
76. Koo BM*, et al.* (2017) Construction and analysis of two genome-scale deletion libraries for *Bacillus subtilis*. *Cell Syst* 4(3):291-305 e297.

bioRxiv preprint doi: https://doi.org/10.1101/2019.12.16.877605; this version posted December 17, 2019. The copyright holder for this preprint (which was not certified by peer review) is the author/funder. All rights reserved. No reuse allowed without permission.

FIGURE LEGENDS

Figure 1: Suppression of the growth defects of a *L. monocytogenes* Δ*gpsB* mutant by *reoM* and *reoY* mutations.

(A-B) Effect of suppressor mutations on growth of the Δ*gpsB* mutant. Growth of *L. monocytogenes* strains EGD-e (wt), LMJR19 (Δ*gpsB*), *shg8* (Δ*gpsB reoY* H87Y), *shg10* (Δ*gpsB reoY* TAA74) and *shg12* (Δ*gpsB reoM* RBS mutation) in BHI broth at 37°C (A) and 42°C (B).

(C-D) Effect of Δ*reoM* and Δ*reoY* deletions on growth of *L. monocytogenes*. Growth of *L. monocytogenes* strains EGD-e (wt), LMJR19 (Δ*gpsB*), LMSW30 (Δ*reoM*), LMSW32 (Δ*reoY*), LMJR137 (Δ*gpsB* Δ*reoM*) and LMJR120 (Δ*gpsB* Δ*reoY*) in BHI broth was recorded at 37°C (C) and 42°C (D). All growth experiments were performed three times and average values and standard deviations are shown.

Figure 2: Effect of the *reoM, reoY* and *clpC* genes on levels of MurA in *L. monocytogenes* and MurAA in *B. subtilis.*

Western blots showing the levels of MurA (above) and DivIVA (as loading controls, middle) in respective *L. monocytogenes* strains, and the quantification of MurA signals (below). Non-relevant lanes were excised from the blots where necessary and average values and standard deviations were calculated from experiments repeated three times. The wild-type value was arbitrarily set to 1 and asterisks indicate statistically significant differences compared to wild type ($P<0.05$, *t*-test) and n. s. means not significant.

(A) Effect of *reoM* and *reoY* deletions (single or when combined with *gpsB* deletion) on MurA levels in *L. monocytogenes* strains EGD-e (wt), LMJR19 (Δ*gpsB*), LMSW30 (Δ*reoM*), LMSW32

bioRxiv preprint doi: https://doi.org/10.1101/2019.12.16.877605; this version posted December 17, 2019. The copyright holder for this preprint (which was not certified by peer review) is the author/funder. All rights reserved. No reuse allowed without permission.

(Δ*reoY*), LMJR137 (Δ*gpsB* Δ*reoM*) and LMJR120 (Δ*gpsB* Δ*reoY*). Strain LMJR138 (Δ*clpC*) was included for comparison.

(B) Effect of *reoM*, *reoY* and *murZ* deletions when combined with *clpC* deletion on MurA levels. MurA levels of *L. monocytogenes* strains EGD-e (wt), LMJR138 (Δ*clpC*), LMJR104 (Δ*murZ*), LMJR171 (Δ*clpC* Δ*murZ*), LMSW30 (Δ*reoM*), LMSW50 (Δ*clpC* Δ*reoM*), LMSW32 (Δ*reoY*) and LMSW51 (Δ*clpC* Δ*reoY*). Strain LMJR123 (I*murA*) grown in the presence or absence of IPTG was included for comparison.

(C) Effect of the *reoM* and *reoY* homologs *yrzL* and *ypiB*, respectively, on MurAA levels of *B. subtilis*. Strains BKE00860 (Δ*clpC*), BKE22180 (Δ*gpsB*), BKE22580 (Δ*ypiB*/*reoY*) and BKE27400 (Δ*yrzL*/*reoM*) were grown to mid-logarithmic growth phase before total cellular proteins were isolated. *B. subtilis* 168 (wt) was included as control. That MurAA is detected in two isoforms had been observed earlier but the reasons for this are not known (26).

Figure 3: The PrkA/PrkP pair controls the phosphorylation status of ReoM.

Non-denaturing PAGE analysis of the phosphorylation (A) and dephosphorylation (B) of ReoM *in vitro*. The components of each lane in the gel is annotated above the image and the position and identity of relevant bands is marked to the side.

(C) LC-MS analysis of intact ReoM. The deconvoluted mass spectrum for non-phosphorylated ReoM (black) is overlaid over the equivalent spectrum for mono-phosphorylated ReoM, P-ReoM (red).

(D) LC-MS/MS was used to perform peptide mapping analysis that revealed that Thr7 is the sole phosphosite of ReoM. The MS/MS fragmentation spectra of the phosphorylated peptide encompassing Asp5-Lys22 is presented with *b*-ion fragmentation in blue and *y*-ion fragmentation shown in red, whilst the precursor ion (m/z 1116.86, z=2+) is represented by a blue diamond.

bioRxiv preprint doi: https://doi.org/10.1101/2019.12.16.877605; this version posted December 17, 2019. The copyright holder for this preprint (which was not certified by peer review) is the author/funder. All rights reserved. No reuse allowed without permission.

Figure 4: A ReoM T7A exchange affects growth and MurA levels in a ClpC-dependent manner. (A) Lethality of the *reoM T7A* mutation in *L. monocytogenes*. *L. monocytogenes* strains EGD-e (wt), LMSW30 (Δ*reoM*), LMSW57 (i*reoM*) and LMSW52 (i*reoM T7A*) were grown in BHI broth ± 1 mM IPTG at 37°C. The experiment was repeated three times and average values and standard deviations are shown. (B) Suppression of *reoM T7A* lethality by deletion of *clpC*. *L. monocytogenes* strains EGD-e (wt), LMJR138 (Δ*clpC*), LMSW52 (i*reoM T7A*) and LMSW72 (i*reoM T7A* Δ*clpC*) were grown in BHI broth ± 1 mM IPTG at 37°C. The experiment was repeated three times and average values and standard deviations are shown. (C) Western blot showing cellular levels of MurA (top) and ClpC (middle) in the strains included in panels A and B. For this experiment, strains were grown in BHI broth not containing IPTG at 37°C. IPTG (1 mM) was added to the cultures at an OD_{600} of 0.2 and the cells were collected 2 hours later. Irrelevant lanes were removed from both blots. Quantification of MurA signals by densitometry is shown below the Western blots. Average values and standard deviations calculated from three independent experiments are shown. Asterisks indicate statistically significant differences ($P<0.05$, *t*-test). (D) Contribution of ReoY and MurZ to the lethal *reoM T7A* phenotype. *L. monocytogenes* strains EGD-e (wt), LMSW52 (i*reoM T7A*), LMSW72 (i*reoM T7A* Δ*clpC*), LMSW123 (i*reoM T7A* Δ*reoY*) and LMSW124 (i*reoM T7A* Δ*murZ*) were grown in BHI broth containing 1 mM IPTG and growth at 37°C was recorded in a microplate reader. Average values and standard deviations were calculated from an experiment performed in triplicate.

Figure 5: Crystal structure of ReoM.

(A) The structure of ReoM depicted as a cartoon with each protomer in the dimer coloured separately (cyan and orange). The secondary structure elements are numbered according to their position in the amino acid sequence. Thr7 and some of the key amino acids in the dimer interface

bioRxiv preprint doi: https://doi.org/10.1101/2019.12.16.877605; this version posted December 17, 2019. The copyright holder for this preprint (which was not certified by peer review) is the author/funder. All rights reserved. No reuse allowed without permission.

885 and the hydrophobic core are drawn as stick figures. (B) Sequence alignment of ReoM (*Lmo*) and
886 its homologues from *Bacillus subtilis* (*Bsu*), *Streptococcus pneumoniae* (*Spn*), *Clostridium*
887 *difficile* (*Cdi*) and *Staphylococcus aureus* (*Sau*) with the sequence of IreB from *Enterococcus*
888 *faecalis* (*Efa*) underneath. Amino acid sequence numbers pertain to ReoM and the site of
889 phosphorylation in ReoM (Thr7) and the twin phosphorylations in IreB (minor site: Thr4; major
890 site: Thr7) are highlighted. Invariant amino acids are shaded black, residues in the ReoM dimer
891 interface have an asterisk above, and the secondary structure elements are defined by cylinders
892 above the alignment. Arginine residues mutated in this study are indicated by an hashtag above
893 the alignment. (C) The final $2F_{obs}$-F_{calc} electron density map, contoured at a level of 0.42 $e^-/Å^3$, of
894 the N-terminal region in the immediate vicinity of Thr7 in chain A of the ReoM dimer indicates
895 that the protein model could be built with confidence even though this region contains no
896 secondary structure elements.
897
898 **Figure 6:** Effect of *prkA* and *prkP* mutations on growth and MurA levels of *L. monocytogenes*.
899 (A) Contribution of PrkA and PrkP to *L. monocytogenes* growth. *L. monocytogenes* strains EGD-
900 e (wt), LMSW76 (Δ*prkP prkA**), LMSW83 (i*prkP*) and LMSW84 (i*prkA*) were grown in BHI
901 broth containing or not containing 1 mM IPTG at 37°C in a microtiter plate reader. The
902 experiment was repeated three times and average values and standard deviations are shown. (B)
903 Contribution of PrkA and PrkP to MurA stability. Western blots showing cellular levels of MurA
904 (top) and DivIVA (middle) in the same set of strains as in panel A and quantification of MurA
905 signals by densitometry (below). Average values and standard deviations calculated from three
906 independent experiments are shown. Asterisks indicate statistically significant differences
907 (P<0.05, *t*-test).
908

bioRxiv preprint doi: https://doi.org/10.1101/2019.12.16.877605; this version posted December 17, 2019. The copyright holder for this preprint (which was not certified by peer review) is the author/funder. All rights reserved. No reuse allowed without permission.

Fig. 7: PrkA essentiality depends on *reoM*, *reoY* and *clpC*.

(A) Effect of *reoM*, *reoY* and *clpC* deletions on *prkA* essentiality. *L. monocytogenes* strains EGD-e (wt), LMSW84 (i*prkA*), LMSW89 (i*prkA* Δ*reoM*), LMSW90 (i*prkA* Δ*reoY*) and LMSW91 (i*prkA* Δ*clpC*) were grown in BHI broth ± 1 mM IPTG at 37°C in a microtiter plate reader. The experiment was repeated three times and average values and standard deviations are shown. (B) *clpC*, *reoM* and *reoY* deletions overcome MurA degradation in PrkA-depleted cells. Western blot showing MurA levels in *L. monocytogenes* strains EGD-e (wt), LMJR138 (Δ*clpC*), LMSW30 (Δ*reoM*), LMSW32 (Δ*reoY*), LMSW84 (i*prkA*), LMSW89 (i*prkA* Δ*reoM*), LMSW90 (i*prkA* Δ*reoY*) and LMSW91 (i*prkA* Δ*clpC*, top). PrkA wild type strains were grown in BHI broth at 37°C to mid-exponential growth phase before protein isolation. A parallel DivIVA Western blot was used as loading control (middle). Quantification of MurA signals by densitometry (below). Average values and standard deviations calculated from three independent experiments are shown. Asterisks indicate statistically significant differences ($P<0.05$, *t*-test).

Fig. 8: ReoM links cell wall integrity sensing with peptidoglycan biosynthesis.

Model illustrating the role of ReoM as substrate of PrkA and as regulator of ClpCP. Cell wall damage is sensed by PrkA through recognition of free muropeptides upon which PrkA phosphorylates ReoM. In its unphosphorlyated form, ReoM is an activator of ClpCP-dependent degradation of MurA, the first enzyme of peptidoglycan biosynthesis, and ReoY and MurZ contribute to this process. By phosphorylating ReoM, PrkA prevents ClpCP-dependent MurA degradation so that MurA accumulates and peptidoglycan biosynthesis can occur. Please note that there is a lesser degree of conservation in the fourth PASTA domain of PrkA.

bioRxiv preprint doi: https://doi.org/10.1101/2019.12.16.877605; this version posted December 17, 2019. The copyright holder for this preprint (which was not certified by peer review) is the author/funder. All rights reserved. No reuse allowed without permission.

932 **Table 1:** Plasmids and strains used in this study

name	relevant characteristics	source*/ reference
Plasmids		
pIMK3	P_{help}-*lacO lacI neo*	(64)
pMAD	*bla erm bgaB*	(67)
pJR127	*bla erm bgaB* Δ*clpC (lmo0232)*	(28)
pSH246	*bla erm bgaB* Δ*gpsB (lmo1888)*	(32)
pJR68	*bla erm bgaB* Δ*murZ (lmo2552)*	(28)
pJR65	P_{help}-*lacO-reoM lacI neo*	this work
pJR70	P_{help}-*lacO-reoY lacI neo*	this work
pJR83	*bla erm bgaB* Δ*reoY (lmo1921)*	this work
pJR126	*bla erm bgaB* Δ*reoM (lmo1503)*	this work
pSW29	P_{help}-*lacO-reoM T7A lacI neo*	this work
pSW36	*bla erm bgaB* Δ*prkA (lmo1820)*	this work
pSW37	*bla erm bgaB* Δ*prkP (lmo1821)*	this work
pSW38	P_{help}-*lacO-prkA lacI neo*	this work
pSW39	P_{help}-*lacO-prkP lacI neo*	this work
pSW55	P_{help}-*lacO-reoM R66A lacI neo*	this work
pSW56	P_{help}-*lacO-reoM R70A lacI neo*	this work
pSW58	P_{help}-*lacO-reoM R57A lacI neo*	this work
pSW59	P_{help}-*lacO-reoM R62A lacI neo*	this work
***B. subtilis* strains**		
168	wild type, lab collection	
BKE00860	Δ*clpC*	(76)
BKE22180	Δ*gpsB*	(76)
BKE22580	Δ*ypiB (reoY)*	(76)
BKE27400	Δ*yrzL (reoM)*	(76)
***L. monocytogenes* strains**		
EGD-e	wild-type, serovar 1/2a strain	(68)
LMJR19	Δ*gpsB (lmo1888)*	(32)
LMJR104	Δ*murZ (lmo2552)*	(28)
LMJR123	Δ*murA (lmo2526) attB::*P_{help}-*lacO-murA lacI neo*	(28)
LMJR138	Δ*clpC (lmo0232)*	(28)
shg8	Δ*gpsB reoY* H87Y	this work
shg10	Δ*gpsB reoY* TAA74	this work
shg12	Δ*gpsB reoM* RBS mutation	this work
LMJR96	Δ*gpsB attB::*P_{help}-*lacO-reoM lacI neo*	pJR65 → LMJR19
LMJR102	*attB::*P_{help}-*lacO-reoM lacI neo*	pJR65 → EGD-e
LMJR106	Δ*gpsB attB::*P_{help}-*lacO-reoY lacI neo*	pJR70 → LMJR19
LMJR120	Δ*gpsB* Δ*reoY*	pJR83 ↔ LMJR19
LMJR137	Δ*gpsB* Δ*reoM*	pJR126 ↔ LMJR19
LMJR171	Δ*clpC* Δ*murZ*	pJR127 ↔ LMJR104
LMSW30	Δ*reoM (lmo1503)*	pJR126 ↔ EGD-e
LMSW32	Δ*reoY (lmo1921)*	pJR83 ↔ EGD-e
LMSW50	Δ*clpC* Δ*reoM*	pJR127 ↔ LMSW30
LMSW51	Δ*clpC* Δ*reoY*	pJR127 ↔ LMSW32
LMSW52	Δ*reoM attB::*P_{help}-*lacO-reoM T7A lacI neo*	pSW29 → LMSW30
LMSW57	Δ*reoM attB::*P_{help}-*lacO-reoM lacI neo*	pJR65 → LMSW30
LMSW72	Δ*reoM attB::*P_{help}-*lacO-reoM T7A lacI neo* Δ*clpC*	pJR127 ↔ LMSW52
LMSW76	Δ*prkP prkA**	pSW37 ↔ EGD-e
LMSW80	*attB::*P_{help}-*lacO-prkA lacI neo*	pSW38 → EGD-e
LMSW81	*attB::*P_{help}-*lacO-prkP lacI neo*	pSW39 → EGD-e
LMSW83	Δ*prkP attB::*P_{help}-*lacO-prkP lacI neo*	pSW37 ↔ LMSW81
LMSW84	Δ*prkA attB::*P_{help}-*lacO-prkA lacI neo*	pSW36 ↔ LMSW80

bioRxiv preprint doi: https://doi.org/10.1101/2019.12.16.877605; this version posted December 17, 2019. The copyright holder for this preprint (which was not certified by peer review) is the author/funder. All rights reserved. No reuse allowed without permission.

name	relevant characteristics	source*/ reference
LMSW89	Δ*prkA attB::*P_{help}-*lacO-prkA lacI neo* Δ*reoM*	pJR126 ↔ LMSW84
LMSW90	Δ*prkA attB::*P_{help}-*lacO-prkA lacI neo* Δ*reoY*	pJR83 ↔ LMSW84
LMSW91	Δ*prkA attB::*P_{help}-*lacO-prkA lacI neo* Δ*clpC*	pJR127 ↔ LMSW84
LMSW117	Δ*reoM* Δ*reoY*	pJR126 ↔ LMSW32
LMSW118	Δ*reoY* Δ*murZ*	pJR68 ↔ LMSW32
LMSW119	Δ*reoM* Δ*murZ*	pJR68 ↔ LMSW30
LMSW120	Δ*reoM attB::*P_{help}-*lacO-reoM R66A lacI neo*	pSW55 → LMSW30
LMSW121	Δ*reoM attB::*P_{help}-*lacO-reoM R70A lacI neo*	pSW56 → LMSW30
LMSW123	Δ*reoM attB::*P_{help}-*lacO-reoM T7A lacI neo* Δ*reoY*	pSW29 → LMSW117
LMSW124	Δ*reoM attB::*P_{help}-*lacO-reoM T7A lacI neo* Δ*murZ*	pSW29 → LMSW119
LMSW125	Δ*reoM attB::*P_{help}-*lacO-reoM R57A lacI neo*	pSW58 → LMSW30
LMSW126	Δ*reoM attB::*P_{help}-*lacO-reoM R62A lacI neo*	pSW59 → LMSW30

* The arrow (→) stands for a transformation event and the double arrow (↔) indicates gene deletions obtained by chromosomal insertion and subsequent excision of pMAD plasmid derivatives (see experimental procedures for details).

bioRxiv preprint doi: https://doi.org/10.1101/2019.12.16.877605; this version posted December 17, 2019. The copyright holder for this preprint (which was not certified by peer review) is the author/funder. All rights reserved. No reuse allowed without permission.

939 **Table 2:** Oligonucleotides used in this study.

name	sequence (5´→3´)
JR163	GCGCCCATGGCTAAGGCATCCATTTCAATAGACGAGAAG
JR164	GCGCGTCGACTTATTCTTTTTCCGTATCCATTTGCTGTA
JR169	GCGCCCATGGATTCAAAAGATCAAACAATGTTTTACAACTTC
JR170	GCGCGTCGACTCATTTCTCACCAATTTCGTTATTTTTCAG
JR197	GCGCGGATCCCAATTATTTCGAATGGTGCGGTGTC
JR198	TCCTTATTCGTCGACCATCTTTCCTCAGTCCCTTCCTG
JR199	GGAAAGATGGTCGACGAATAAGGAATAAATCCTAGTTAGTAGGG
JR200	CGCGCGAATTCCCAAGACTCAACCTCTTTCACTC
JR264	GCGCAGATCTGGCAAATACAGCATTGAACTATGTG
JR265	GCGCGGATCCAATCGAAGCACCTCATTCCTTC
JR266	GCGCGGATCCATGAGAATAATGGGTTTAGATGTCGGC
JR267	GCGCGTCGACGCTAGGAATGTAGCAAGGATTTCTTC
SHW815	GATCTATCGATGCATGCCATGGGCTAAATGACCAAGGAATTACCG
SHW816	CGCGTCGGGCGATATCGGATCCTTTCTTCCGCGTTTTGGTAACG
SHW817	CAATCATCATTTTAAAAGCACCTCACTATTTTTCAG
SHW818	TGCTTTTAAAATGATGATTGGTAAGCGATTAAGC
SHW819	GATCTATCGATGCATGCCATGGAGATAGAGGCAGAATAAGACATC
SHW820	CGCGTCGGGCGATATCGGATCCGGTATTTACAACCACTACGTCG
SHW821	CGTTCTTATTTCATGAAGCATCCCTCCCTTTC
SHW822	TGCTTCATGAAATAAGAACGGAGGAAATGTGCTG
SW77	GTAAAACATTGCTTGATCTTTTGAATCCATGGGTTTCAC
SW78	GATCAAGCAATGTTTTACAACTTCGGCGATGATTC
SW110	GCGCGCGGATCCATGCATGCAGAATTTAGAACAGATAG
SW111	GCGCGCGTCGACTCATGAAGCATCCCTCCCTTTC
SW112	GCGCGCGGATCCATGATGATTGGTAAGCGATTAAGCG
SW113	GCGCGCGTCGACTTAATTTGGATAAGGGACTGTACCTTC
SW136	CTAAACGAGCTATCATACTTCTAGCATCCTTGTGAC
SW137	GTATGATAGCTCGTTTAGAACGAGATGAAATTATCGAG
SW138	AATTTCATCTGCTTCTAAACGACGTATCATACTTCTAGC
SW139	GTTTAGAAGCAGATGAAATTATCGAGGAACTTGTCAAAG
SW144	CCTTGTGAGCAGGAATATAAGCAGGATCGCCTG
SW145	TATATTCCTGCTCACAAGGATGCTAGAAGTATGATAC
SW146	GTATCATACTTGCAGCATCCTTGTGACGAGGAATATAAG
SW147	GGATGCTGCAAGTATGATACGTCGTTTAGAACGAG
Lmo1503F	GCTATACCATGGATTCAAAAGATCAAACAATGTTTTACAAC
Lmo1503R	CGATATCTCGAGTCATTTCTCACCAATTTCGTTATTTTTCAG
PrkAF	GCTATACCATGGCAATGATGATTGGTAAGCGATTAAGCG
PrkAR	CGATATCTCGAGTCATTTTTTCTTTTTCTTATCTTTTTTCTCCTCAGG
PrkPF	GCTATACCATGGCAATGCATGCAGAATTTAGAACAGATAGAG
PrkPR	CGATATCTCGAGTCATGAAGCATCCCTCCCTTTC

940

941

bioRxiv preprint doi: https://doi.org/10.1101/2019.12.16.877605; this version posted December 17, 2019. The copyright holder for this preprint (which was not certified by peer review) is the author/funder. All rights reserved. No reuse allowed without permission.

942 **Table 3:** Summary of the data collection and refinement statistics for ReoM.

Data collection	
Beamline	Diamond I03
Wavelength (Å)	0.976
Resolution (Å)	74.45-1.60 (1.63-1.60)*
Space group	P 2_1 2_1 2_1
a, *b*, *c* (Å)	38.79, 58.62, 74.45
α, β, γ (°)	90, 90, 90
R_{pim}	0.064 (0.533)
CC (1/2) (%)	98.6 (62.0)
<I>/<σ(I)>	8.2 (2.2)
Completeness (%)	99.8 (99.8)
Redundancy	4.8 (4.9)
Total observations	111229 (5581)
Unique reflections	23059 (1129)
Refinement	
R_{work} (%)	15.3
R_{free} (%)	21.4
Solvent content (%)	38.0
# atoms	
Protein	1399
Ligand/ion	20
Water	94
B-factors (Å^2)	
Protein	26.4
Ligand/ion	50.5
Water	37.7
R.m.s deviations	
Bonds (Å)	0.015
Angles (°)	1.79

943 *Where values in parentheses refer to the highest resolution shell.

944

945

946

bioRxiv preprint doi: https://doi.org/10.1101/2019.12.16.877605; this version posted December 17, 2019. The copyright holder for this preprint (which was not certified by peer review) is the author/funder. All rights reserved. No reuse allowed without permission.

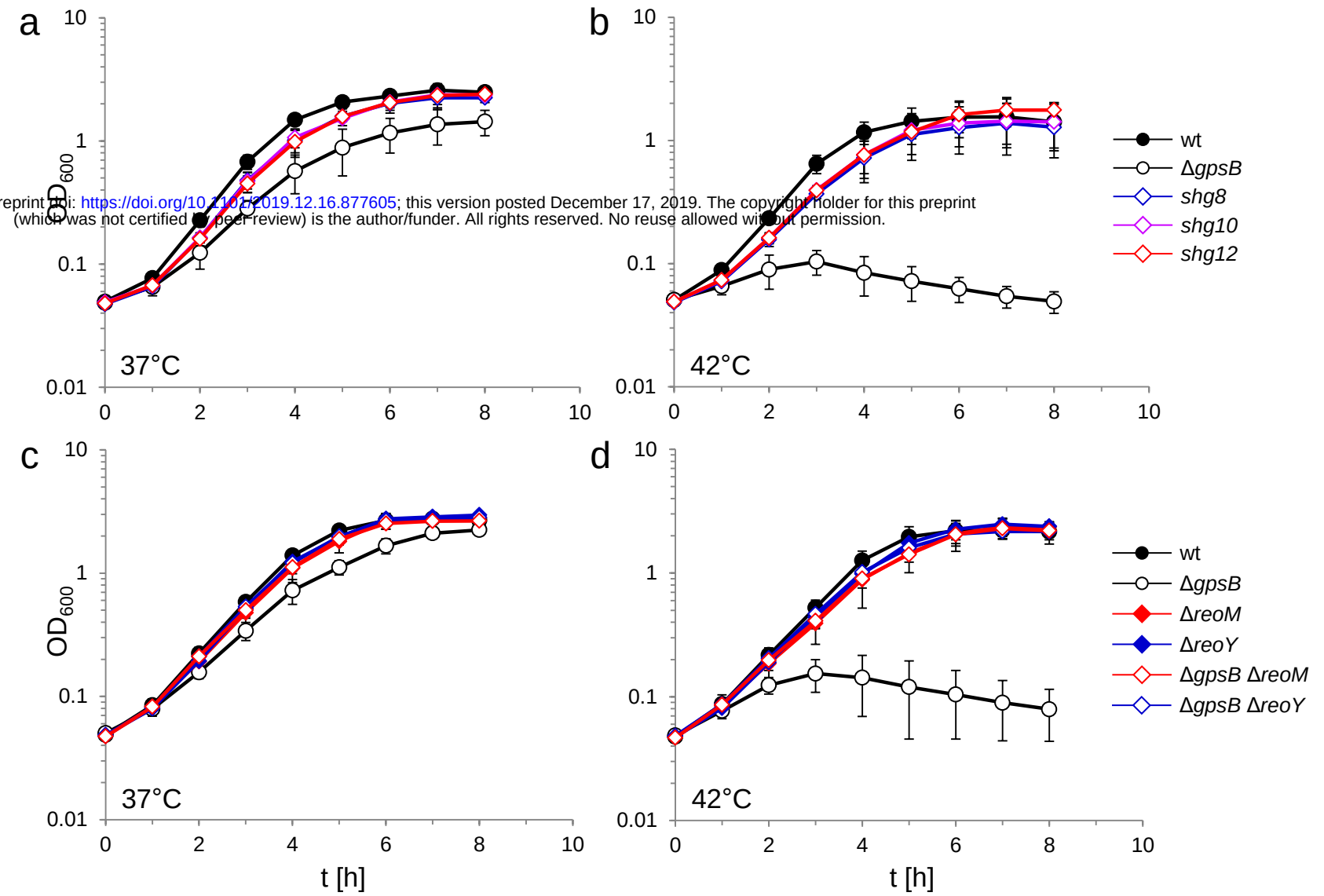

Wamp *et al.*, Fig. 1

bioRxiv preprint doi: https://doi.org/10.1101/2019.12.16.877605; this version posted December 17, 2019. The copyright holder for this preprint (which was not certified by peer review) is the author/funder. All rights reserved. No reuse allowed without permission.

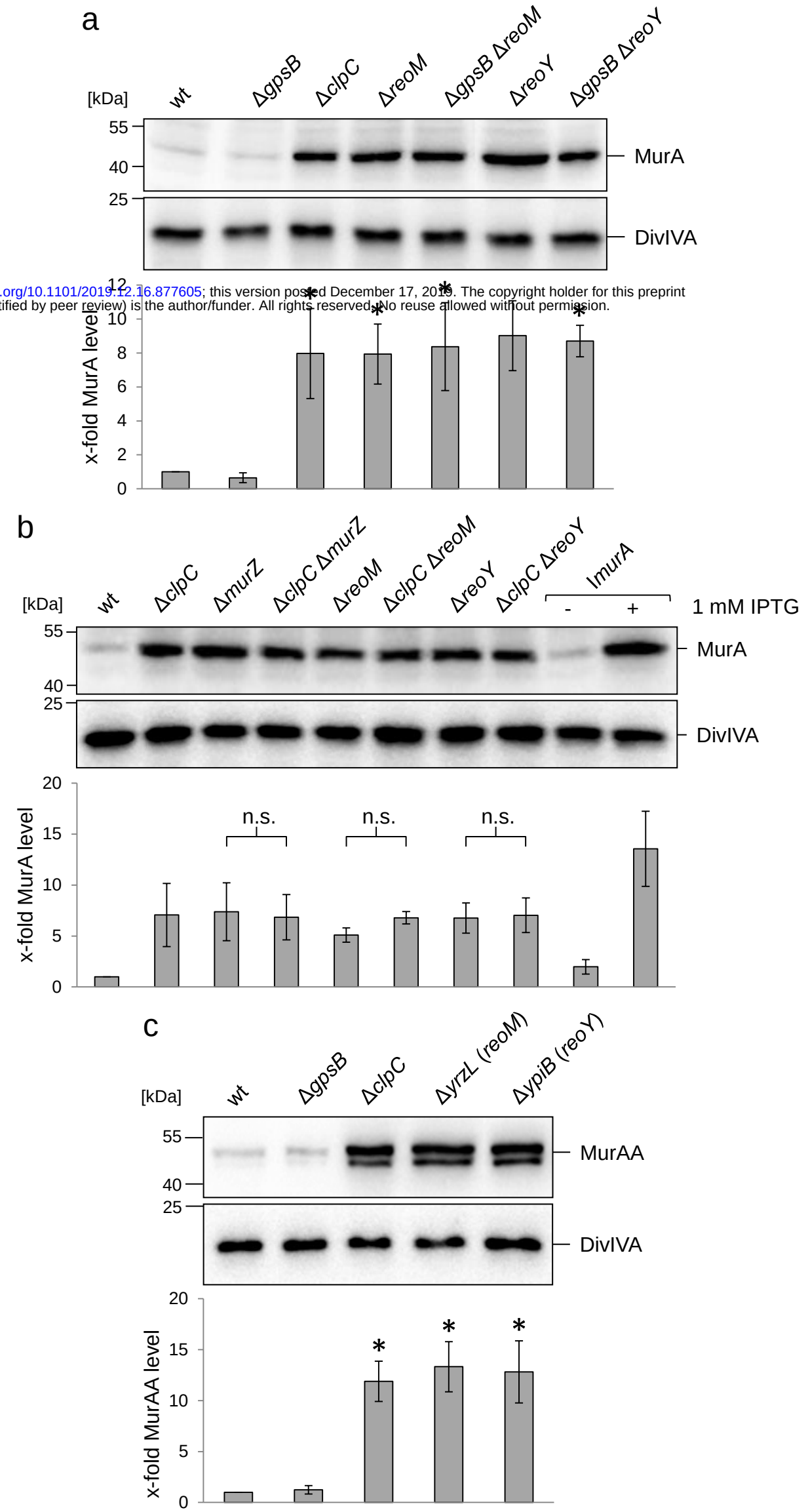

Wamp *et al.*, Fig. 2

bioRxiv preprint doi: https://doi.org/10.1101/2019.12.16.877605; this version posted December 17, 2019. The copyright holder for this preprint (which was not certified by peer review) is the author/funder. All rights reserved. No reuse allowed without permission.

a

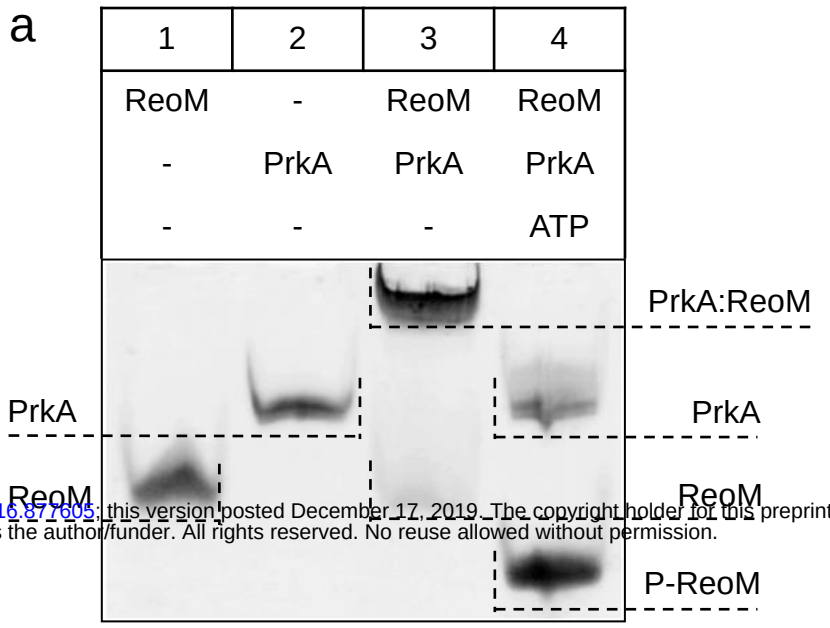

b

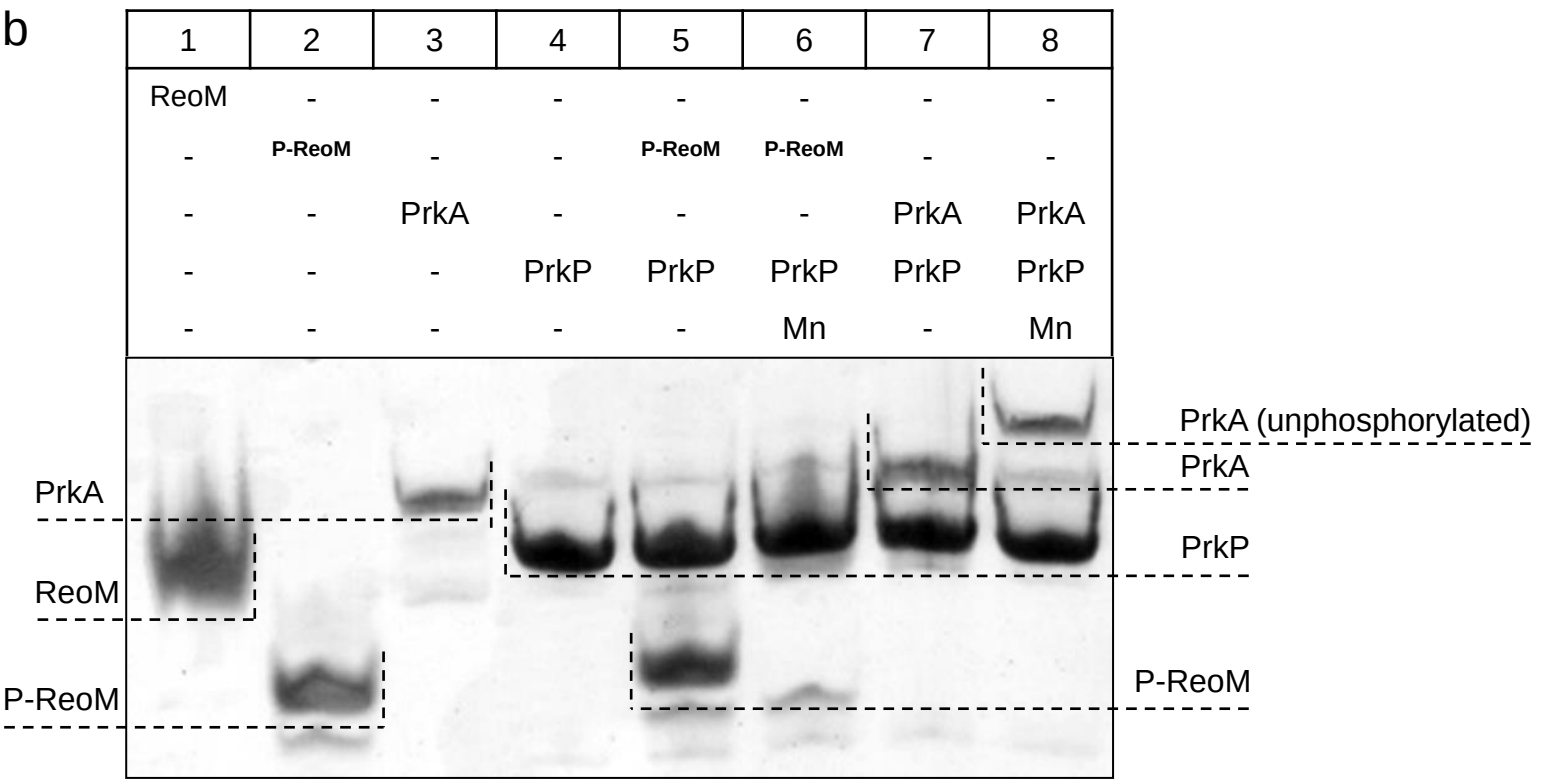

c

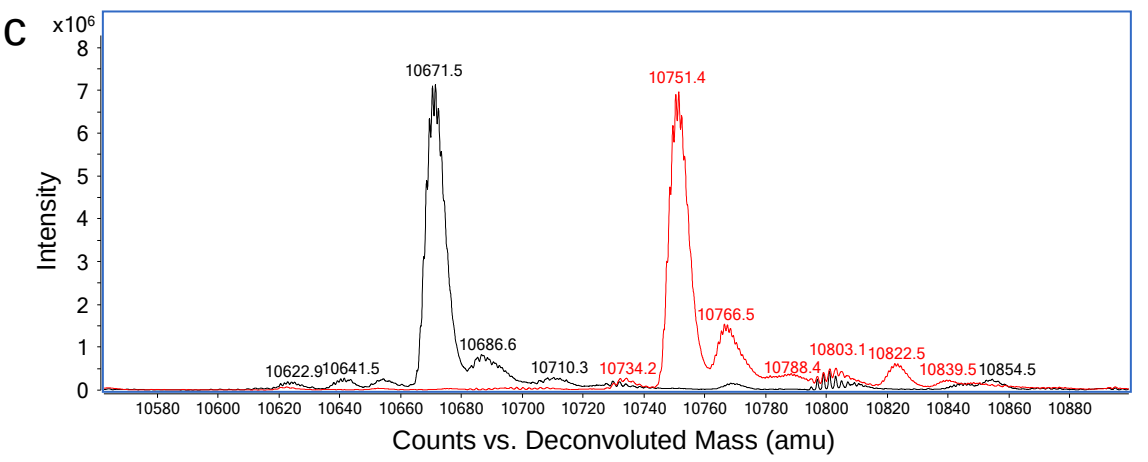

d

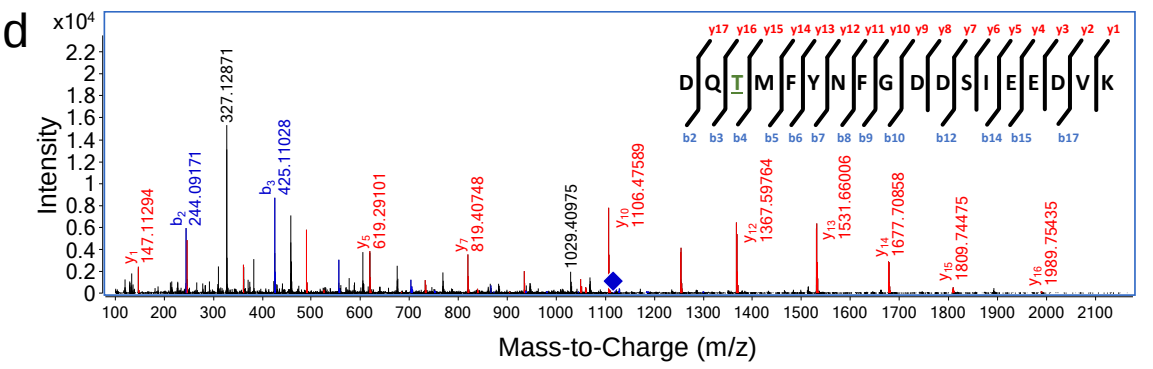

Wamp *et al.*, Fig. 3

bioRxiv preprint doi: https://doi.org/10.1101/2019.12.16.877605; this version posted December 17, 2019. The copyright holder for this preprint (which was not certified by peer review) is the author/funder. All rights reserved. No reuse allowed without permission.

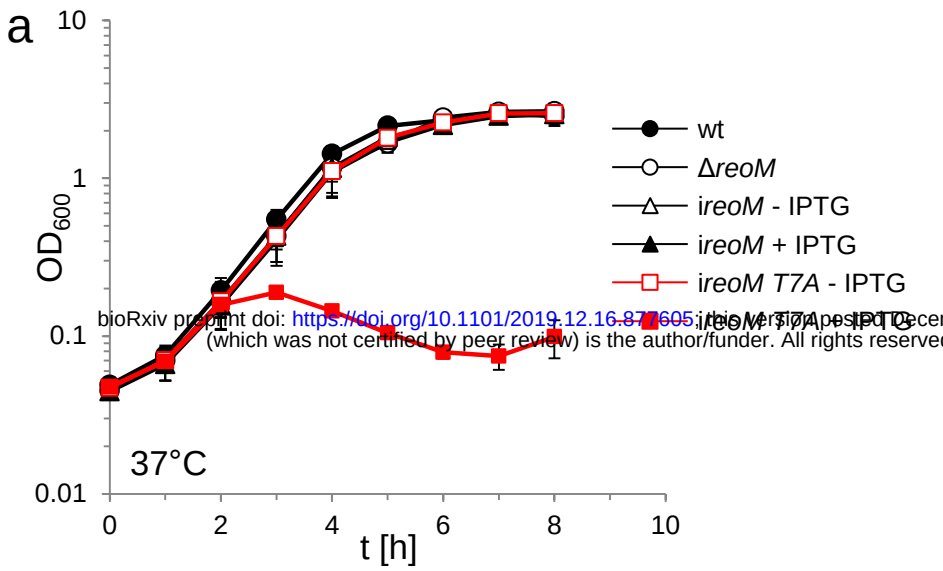

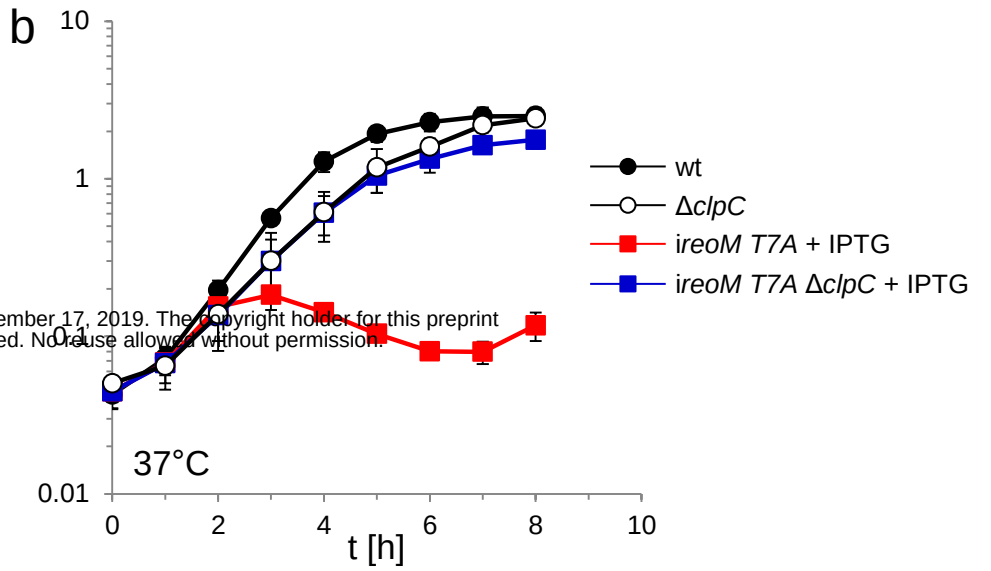

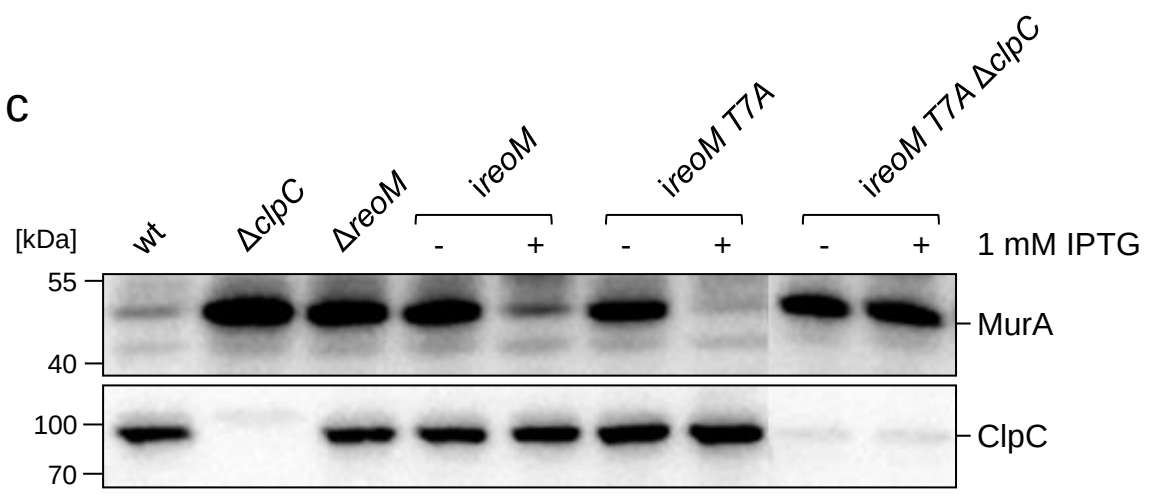

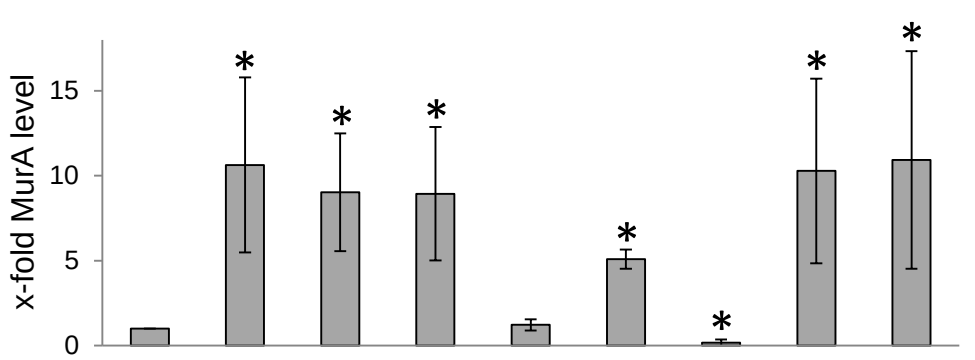

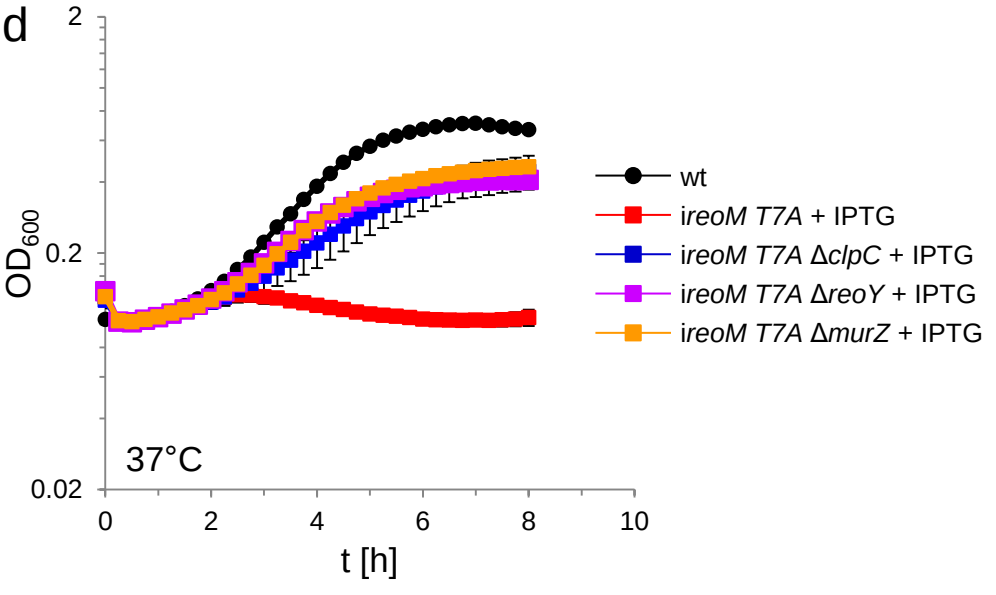

Wamp *et al.*, Fig. 4

bioRxiv preprint doi: https://doi.org/10.1101/2019.12.16.877605; this version posted December 17, 2019. The copyright holder for this preprint (which was not certified by peer review) is the author/funder. All rights reserved. No reuse allowed without permission.

a

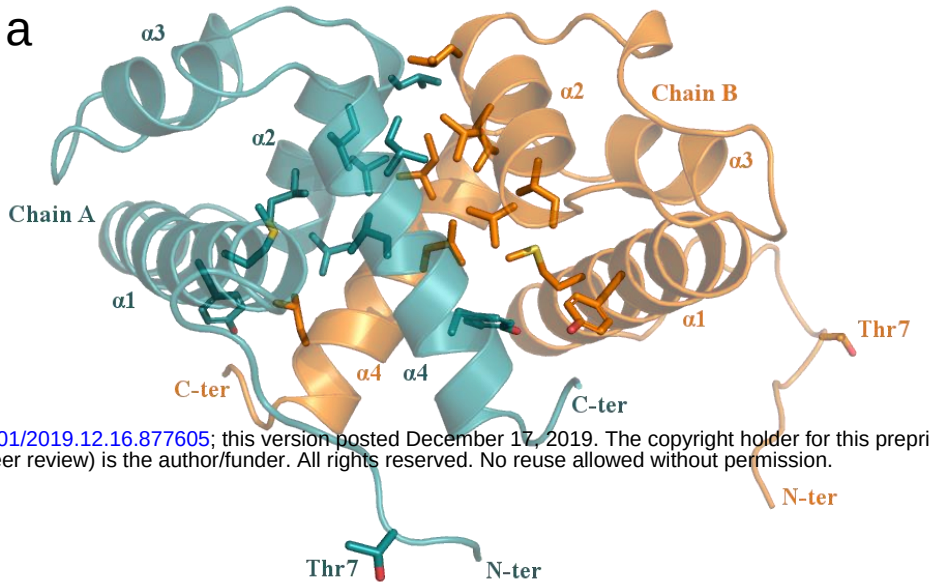

b

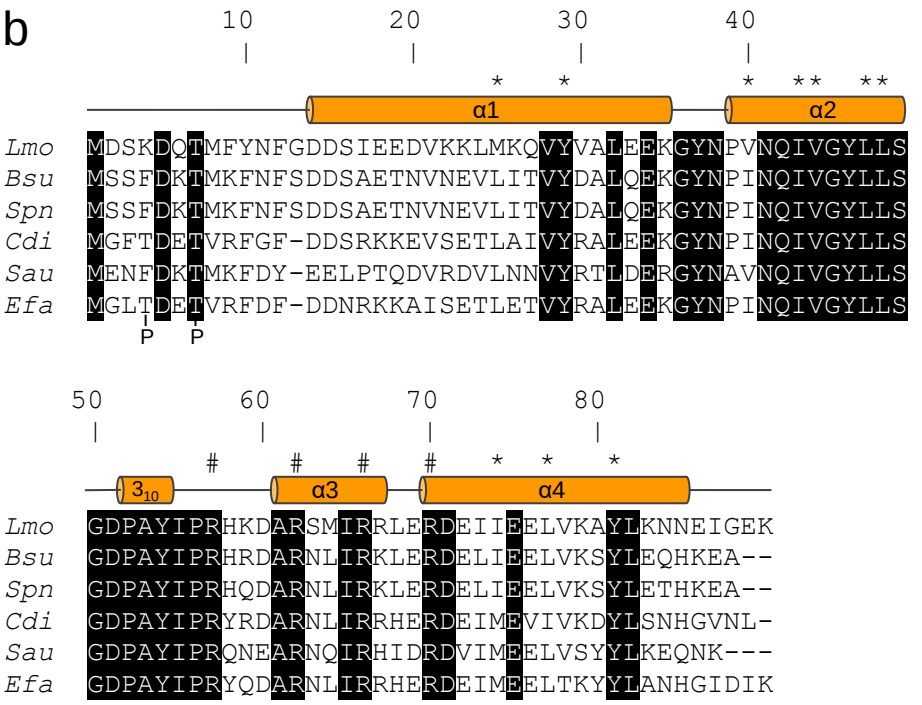

c

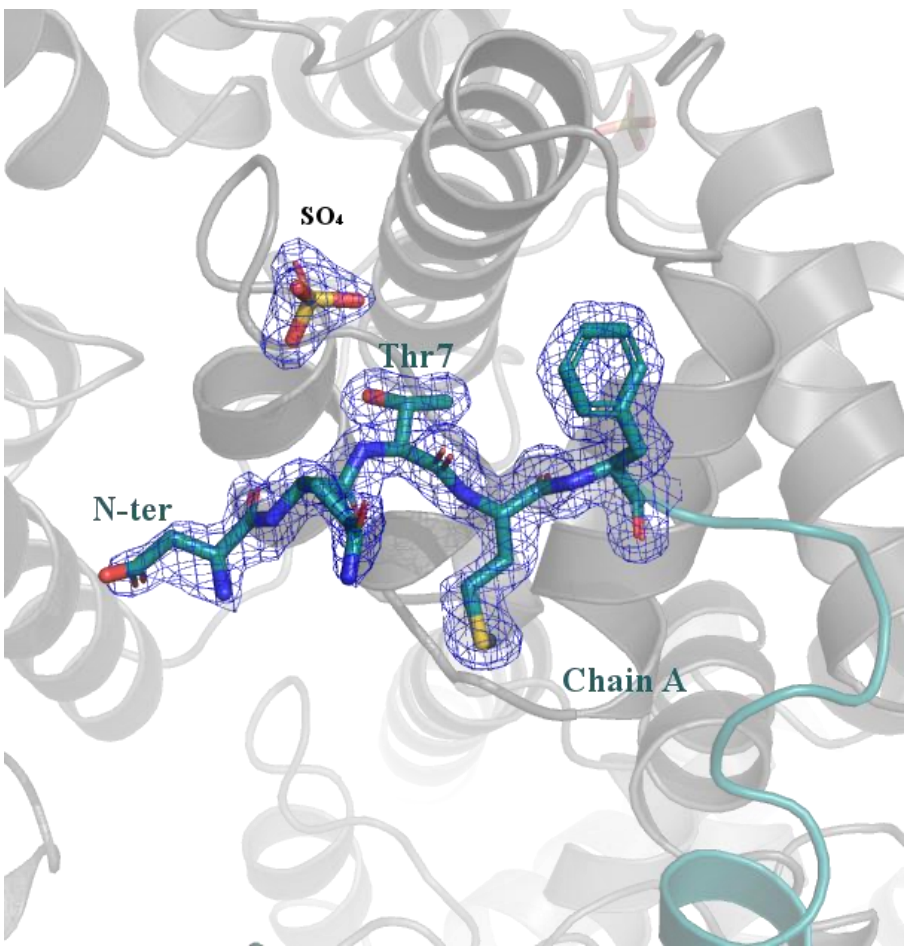

Wamp *et al.*, Fig. 5

bioRxiv preprint doi: https://doi.org/10.1101/2019.12.16.877605; this version posted December 17, 2019. The copyright holder for this preprint (which was not certified by peer review) is the author/funder. All rights reserved. No reuse allowed without permission.

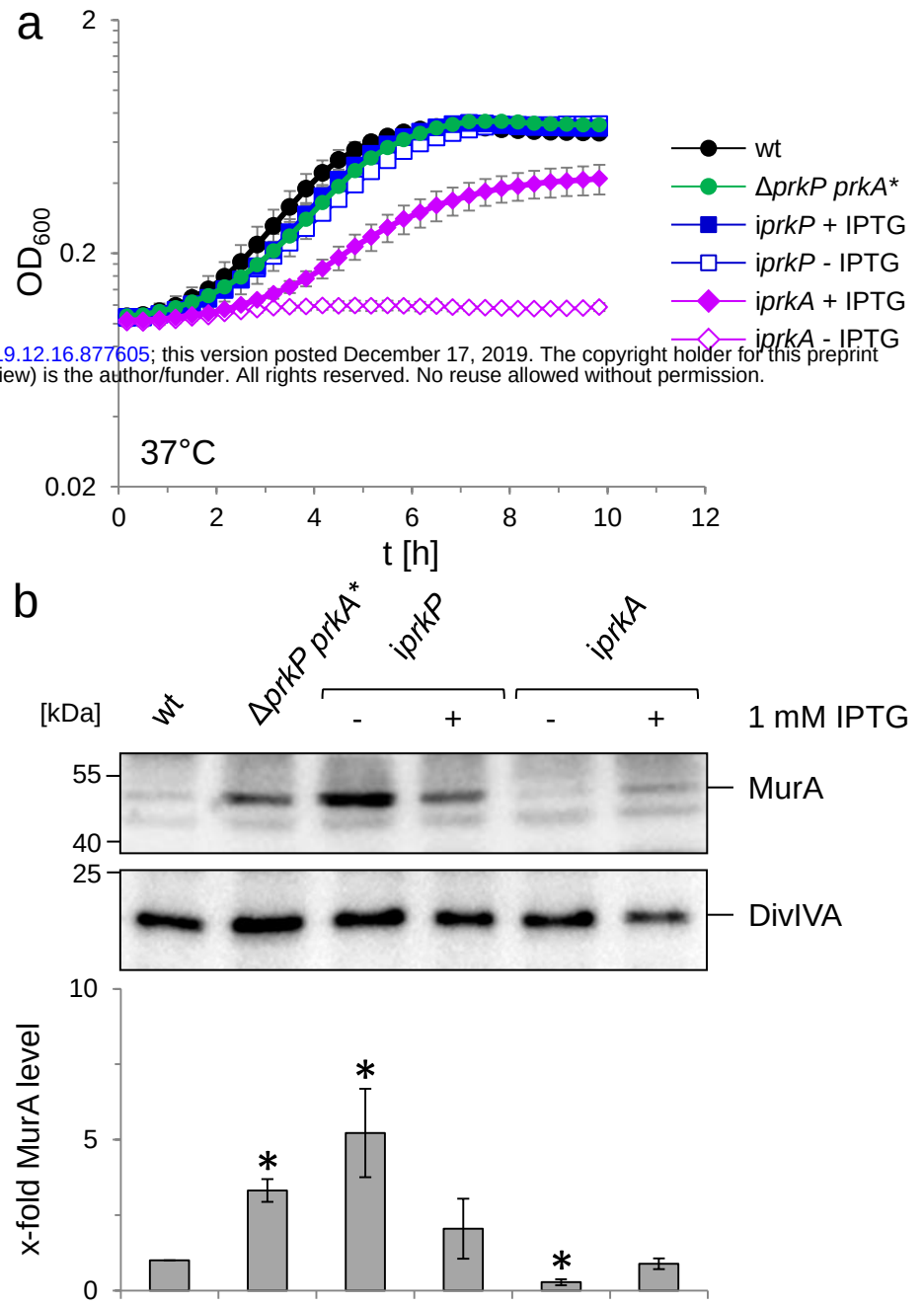

Wamp *et al.*, Fig. 6

bioRxiv preprint doi: https://doi.org/10.1101/2019.12.16.877605; this version posted December 17, 2019. The copyright holder for this preprint
(which was not certified by peer review) is the author/funder. All rights reserved. No reuse allowed without permission.

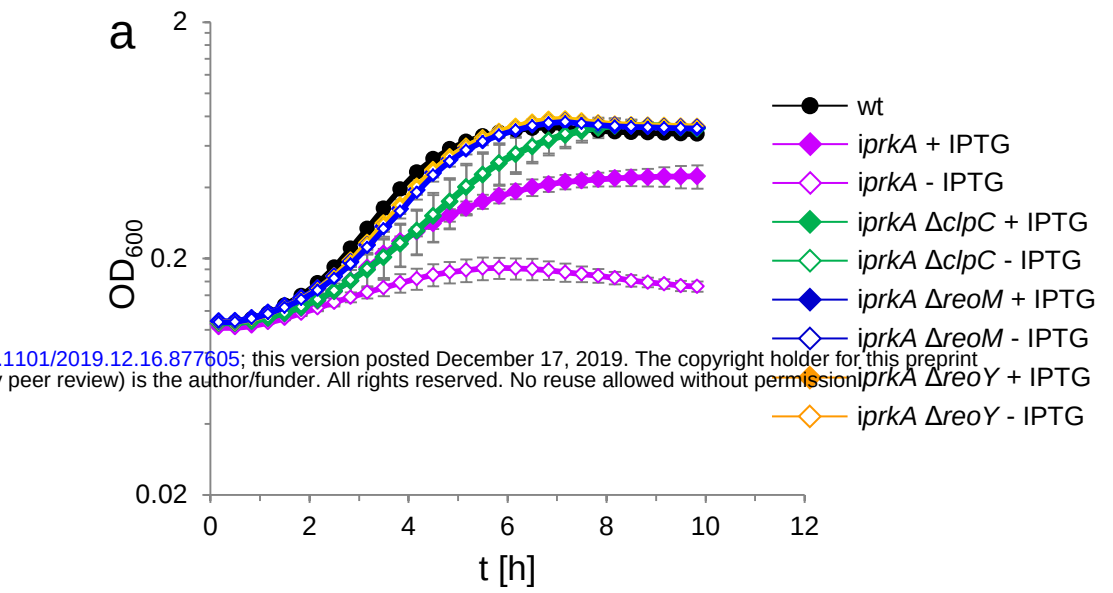

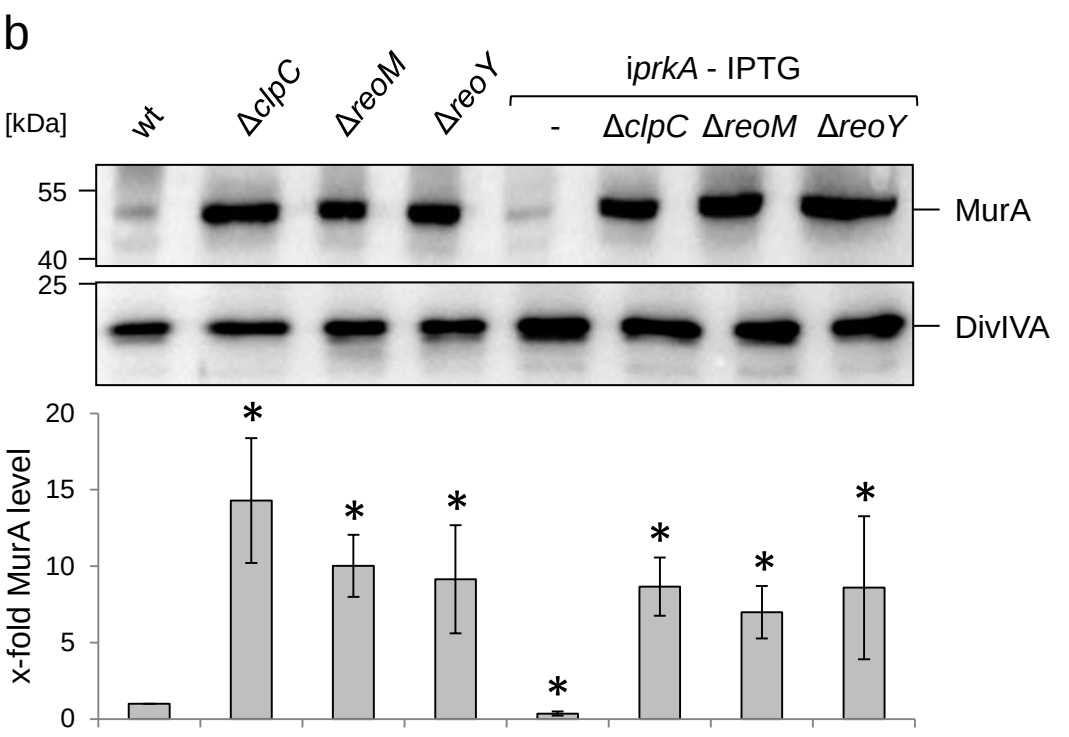

Wamp *et al.*, Fig. 7

bioRxiv preprint doi: https://doi.org/10.1101/2019.12.16.877605; this version posted December 17, 2019. The copyright holder for this preprint (which was not certified by peer review) is the author/funder. All rights reserved. No reuse allowed without permission.

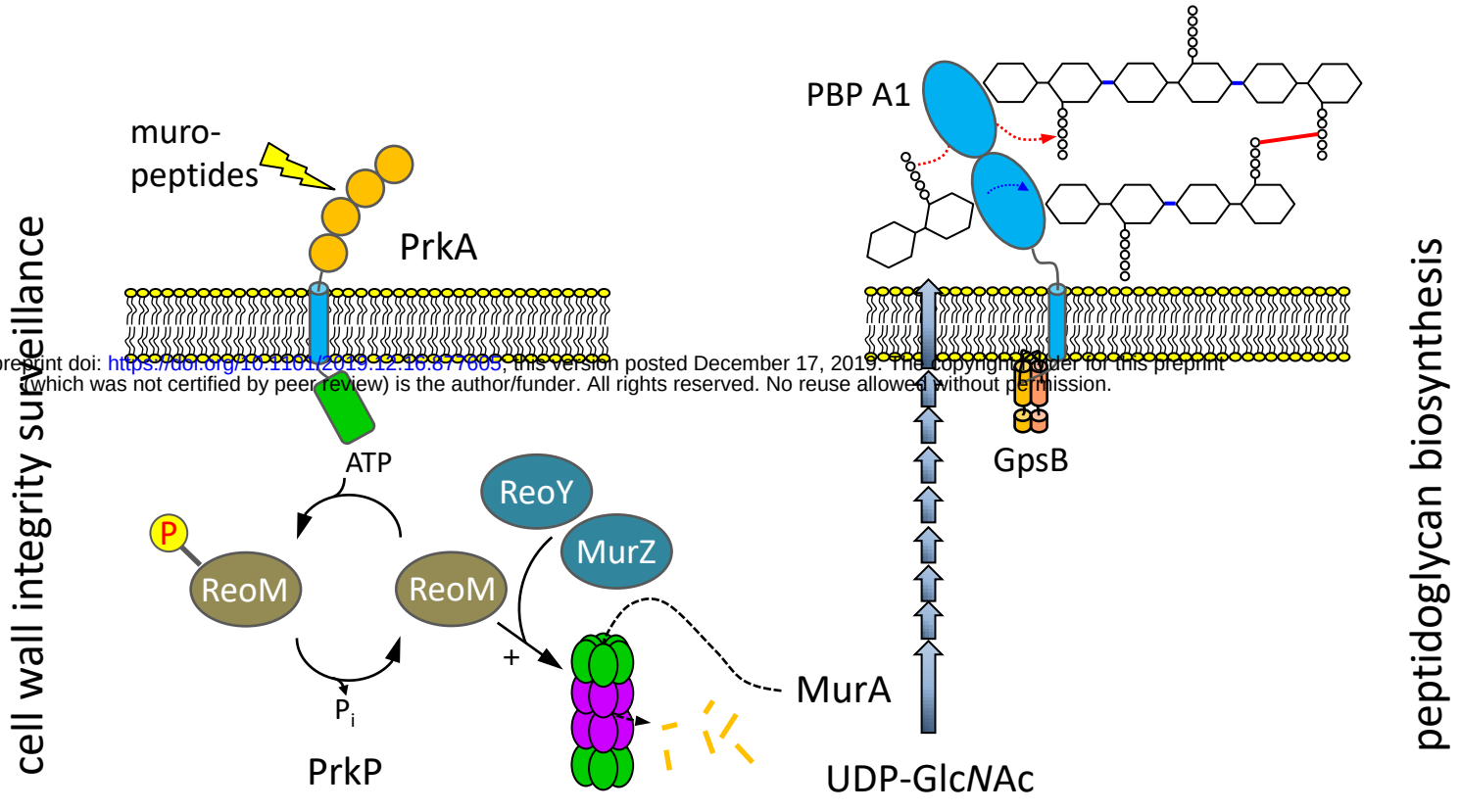

Wamp *et al.*, Fig. 8